Discovery, *in-vitro* and *in-vivo* efficacy of an anti-inflammatory small molecule inhibitor of C-reactive protein

Johannes Zeller
Medical Center - University of Freiburg
Karen Cheung Tung Shing
Department of Biochemistry and Pharmacology, Bio21 Molecular Science and Biotechnology Institute, The University of Melbourne, Parkville, Victoria, Australia
Tracy Nero
University of Melbourne https://orcid.org/0000-0002-3393-1843
Guy Krippner
Baker Heart and Diabetes Institute, Melbourne, Victoria, Australia
James McFadyen
Baker Heart and Diabetes Institute
Balazs Bogner
Medical Center - University of Freiburg
Sheena Kreuzaler
University Heart Center Freiburg
Jurij Kiefer
Medical Center - University of Freiburg https://orcid.org/0000-0002-1008-4522
Verena Horner
Medical Center - University of Freiburg
David Braig
University of Freiburg Medical Center
Michel Kather
University of Freiburg
Bernd Kammerer
Albert-Ludwigs-University Freiburg
Kevin Woollard
Imperial College London https://orcid.org/0000-0002-9839-5463
Prerna Sharma
Baker Heart and Diabetes Institute
Craig Morton
University of Melbourne

Geoffrey Pietersz
The University of Melbourne
Michael Parker
University of Melbourne
Karlheinz Peter
Atherothrombosis and Vascular Biology Laboratory, Baker Heart and Diabetes Institute, Melbourne
Steffen Eisenhardt (steffen.eisenhardt@uniklinik-freiburg.de)
Medical Center - University of Freiburg

Article

Keywords: mCRP, CRP activation, pCRP

Posted Date: October 6th, 2021

DOI: https://doi.org/10.21203/rs.3.rs-944388/v1

Abstract

C-reactive protein (CRP) is an acute phase protein. We recently identified a novel mechanism that leads to a conformational change from the native, pentameric structure (pCRP) to a pentameric intermediate (pCRP*) and ultimately to the monomeric form, mCRP, both being highly pro-inflammatory. This 'CRP activation' is mediated by binding of pCRP to activated/damaged cell membranes via exposed phosphocholine (PC) lipid head groups. We designed a low molecular weight pCRP – PC inhibitor, C10M. Binding assays and X-ray crystallography revealed direct, competitive binding of C10M to pCRP, blocking interaction with PC and thereby inhibiting formation of pCRP*/mCRP and their pro-inflammatory effects. The anti-inflammatory potential of C10M was confirmed *in-vitro* by various measures of leukocyte and endothelial cell activation and *in-vivo* in rat models of acute ischemia/reperfusion injury and hindlimb transplantation. In conclusion, inhibition of pCRP*/mCRP generation via the PC-mimicking compound C10M represents a promising, potentially broadly applicable anti-inflammatory therapy.

Introduction

C-reactive protein (CRP) is an acute phase protein that is synthesized in the liver under the regulation of the cytokine interleukin 6 (IL-6) and circulates as a disc-shaped homo-pentamer (pCRP) [1]. Whilst pCRP itself is not pro-inflammatory when injected into healthy individuals [2], it amplifies tissue injury in the context of inflammation and ischemia [3]. Animal models of myocardial infarction [4,5], stroke [6] and ischemia/reperfusion injury (IRI) [7,8] have demonstrated that pCRP administration can significantly increase tissue injury [3]. Previously, we identified a novel mechanism that can be viewed as a pro-inflammatory 'CRP-activation' process [9,10]. In the context of inflammation and tissue damage, membrane changes on activated cell membranes mediated by phospholipase A2 [11] lead to the exposure of bioactive lipids. This results in the binding of circulating pCRP and subsequent changes in CRP conformation from the pentameric structure (pCRP) to a partially dissociated pentamer (pCRP*) and ultimately in dissociation to its monomeric form (mCRP) [9,12,13]. pCRP* and mCRP are strong pro-inflammatory agents, and can induce IL-8 secretion in neutrophils[14] and human coronary artery endothelial cells [15], promote neutrophil-endothelial cell adhesion [16], and delay apoptosis of human neutrophils [17]. pCRP* can also bind and activate complement C1q [13], which further contributes to aggravation of pre-existing inflammation and detrimental tissue damage [9,11].

Phosphocholine (PC) and phosphoethanolamine (PE) head groups of bioactive lipids are exposed on the surface of activated and damaged cells. Both head groups are known to bind to a shallow groove containing two Ca^{2+} cations located on one face of the monomeric subunit of pCRP, hence there are 5 PC/PE binding pockets on the same face of the CRP pentamer. The concept of targeting the PC/PE binding pockets of pCRP with a synthetic ligand was first explored by Pepys *et al* [4], when they synthesized and evaluated palindromic compounds comprising two molecules of PC covalently linked through one of the phosphate oxygen atoms by a flexible carbon-based linker; one such compound was 1,6-bis(phosphocholine)-hexane (bis-PC, molecular weight ~ 450 Da). It was demonstrated by X-ray

crystallography that each of the PC head groups of bis-PC binds to two separate CRP pentamers, and when multiple bis-PC molecules bind they bring the PC-binding surfaces of the two pentamers together in a parallel fashion. By binding in this manner, palindromic compounds like bis-PC prevent pCRP from interacting with bioactive lipids on activated/damaged cell surfaces thereby blocking the formation of pCRP* and mCRP. As CRP has a central role in many inflammatory reactions and diseases it represents an attractive therapeutic target. Helical polypeptides with covalently attached (via a carbon-based linker) PC molecules [18], peptide mimetics (molecular weight > 700 Da) [19] and anti-sense oligonucleotides [20] targeting CRP have also been developed, with only the latter reaching phase II clinical trials (ISIS-329993 and ISIS-353512, NCT01710852, NCT01414101 and NCT00734240) [21]. Furthermore, reducing circulating pCRP levels via CRP-apheresis using PC-linked resins is currently being investigated as an adjunct therapy to minimize cardiac injury in patients with myocardial infarction [22]. The therapeutic approaches discussed above target general pCRP inhibition and reduction of circulating pCRP levels. However, such approaches come at the cost of some level of immune suppression, which can potentially lead to significant side effects.

We hypothesized that we could design a low molecular weight compound that targets the PC/PE binding pocket on pCRP and thereby prevent the formation of the pro-inflammatory pCRP* and mCRP species. As proof of concept we present the data for C10M, (3-(dibutylamino)propyl)phosphonic acid, a pCRP*/mCRP inhibitor with a molecular weight of just 250 Da. After confirming that C10M bound to the PC/PE binding pocket of pCRP using X-ray crystallography and biophysical techniques, we investigated the therapeutic potential of this compound in various *in-vitro*, *ex-vivo* and *in-vivo* experimental models of inflammation. We analyzed its mode of action and demonstrated that C10M prevents pCRP from binding to activated or damaged cell membranes, thereby blocking the formation of the pro-inflammatory pCRP* and mCRP species. Furthermore, we tested the immunosuppressive impact of C10M on the CRP-dependent innate immune response to bacterial pathogens to preserve protective capacities against *Streptococcus pneumoniae* (*S. pneumoniae*) in order to present a targeted therapy against exacerbated inflammation. Overall, we generated and characterized a PC-mimicking compound that inhibits the generation of pro-inflammatory pCRP*/mCRP and represents a promising, potentially broadly applicable therapeutic for the many patients suffering from inflammatory diseases.

Results

Design of the pCRP*/mCRP inhibitor C10M

To design a proof of concept inhibitor, we felt it was important to retain the interactions made by the PC/PE head groups of bioactive lipids to pCRP. The PC/PE binding pockets are located on what is designated as the B-face of the disc-shaped CRP pentamer [13]. Once bound, the lipid PC/PE head groups anchor the pCRP protein to the damaged cell surface, which then initiates the conformational change to pCRP* and ultimately mCRP [13]. The face of the CRP pentamer not containing the PC/PE binding pockets is known as the A-face and is not involved in binding to activated/damaged cell membranes. PC is

anchored to the shallow groove on the B-face of pCRP monomers via (1) a salt bridge interaction between the positively charged quaternary amine and the negatively charged carboxyl group of Glu 81 and (2) coordination of the negatively charged phosphate moiety to the positively charged Ca^{2+} cations (Fig. 1A). In addition, pCRP residues Asn 61 and Gln 150 lie on opposite sides of the binding pocket and their side-chains participate in hydrogen bonds with oxygen atoms of the PC phosphate moiety, while the other residues lining the binding pocket contribute hydrophobic interactions only (the full list of interacting pCRP residues is given in Table S1). The low molecular weight compound C10M (250 Da, Fig. 1A) was intended to mimic the anchoring interactions of PC. To retain the critical coordination to the Ca^{2+} cations, whilst removing susceptibility to serum nuclease activities, the PC phosphate moiety was replaced with a phosphonate. To take advantage of the space in the binding pocket near the PC quaternary amine (indicated by the vectors R1 and R2, Fig. 1A), we replaced the methyl substituents of PC with n-butyl groups and reverted to a tertiary amine to mitigate any steric hindrance to accessing Glu 81 that the longer n-butyl groups may cause. C10M was synthesized by a two-step synthetic method from commercially available precursors in reasonable yield (Supplementary Materials and Methods) and evaluated for its binding affinity for pCRP.

C10M binds to pCRP in-vitro

The binding of C10M to pCRP was investigated using surface plasmon resonance (SPR). The pCRP was immobilized on the sensor chip using amine coupling and different concentrations of the C10M compound were injected (Fig. 1B, top panel). The relative responses (RU), after corrections for a blank surface and buffer, indicated a binding affinity (K_D) of 105 ± 12 μM for C10M to pCRP (Fig. 1B, bottom panel). In comparison, PC (positive control compound) reported a K_D of 4.0 ± 0.6 μM using the same SPR protocol (data not shown), which is consistent with previous studies by Christopeit *et al*. [23]. These biophysical data confirmed a direct binding of C10M to pCRP. The ability of C10M to inhibit the binding of pCRP to the physiological ligand PC was analyzed using immobilized PC-KLH by ELISA. In this assay C10M had an IC_{50} of 1.5 ± 0.3 mM (data not shown). The inhibitory effect of C10M was further investigated using PC immobilized on agarose beads. C10M (43.5 μg/ml) reduced binding of pCRP (200 μg) to these beads by ~ 70 % (Fig. 1C).

To determine the mode of binding of compound C10M to pCRP, co-crystallization experiments were undertaken and the structure of the complex was solved using X-ray crystallography at a resolution of 3.5 Å (see Table S2 for statistics and Fig. S1). The asymmetric unit consisted of four CRP pentamers with the A-faces stacked against each other (Fig. 1D). Each pCRP monomeric unit adopted a similar fold to that previously published for the PC:pCRP complex (PDB ID: 1B09 [24]), with a root mean square deviation of 0.5 Å over all Cα atoms upon alignment. Only five of the pCRP monomers within the asymmetric unit had a C10M molecule bound. The location of the C10M molecules confirmed that the compound binds to the PC/PE binding pocket, with the phosphonate moiety being the main mediator of the interaction with pCRP via the Ca^{2+} cations (Fig. 1D - F). Residues Asn 61 and Gln 150 are in hydrogen bonding distance of oxygen atoms of the C10M phosphonate moiety, as observed in the PC:pCRP complex (PDB ID: 1B09 [24],

Fig. 1A and E, Table S1). In contrast to the positively charged quaternary amine of PC, the tertiary amine of C10M does not appear to interact with Glu 81 via a hydrogen bond, rather the interactions with this residue are hydrophobic (Table S1). The n-butyl amine substituents of C10M make numerous hydrophobic contacts with pCRP residues (a full list of putative interacting pCRP residues is given in Table S1). Upon alignment of all five pCRP monomers with a bound C10M molecule, it is evident that while the phosphonate moiety anchors the compound into the pocket by interacting with the Ca^{2+} cations, there is a wide variation in the binding orientation of the C10M alkyl backbone and the n-butyl amine substituents (Figs. 1G and S1).

C10M inhibits pCRP binding to activated cell membranes

Activated platelet membranes expose the PC head groups of lysophosphatidylcholine (LPC) and thereby mediate the conformational changes of CRP [9,12,25,26]. We have previously demonstrated that pCRP binds to activated cell membranes but not to membranes of healthy cells [13]. After 120 min bound to activated cell membranes, pCRP begins to dissociate to the pro-inflammatory pCRP* species; however, the proportion of pCRP* is greatest on the surface of microvesicles released by damaged cells. To investigate whether C10M binding to pCRP is sufficient to inhibit the pro-inflammatory effects of CRP, we determined the ability of C10M to prevent pCRP binding to activated platelets. Binding of fluorescently labeled (Atto 594, λ_{ex} 601nm λ_{em} 627nm, Sigma-Aldrich) human pCRP on isolated and ADP-stimulated platelets was investigated by flow cytometry (Fig. 2A). When incubated with C10M, significantly less pCRP-Atto 594 bound to activated platelets. Controls showed Ca^{2+}-dependent binding of pCRP-Atto 594 to platelets (Fig. S2). Flow cytometric results were visualized and confirmed by confocal laser scanning microscopy (Fig. 2B). This was further confirmed by Western blotting of activated platelets that were incubated with either pCRP alone or pCRP + C10M. After washing steps, only a small fraction of CRP could be detected by Western blot in the presence of C10M, whereas significant amounts of CRP were detectable in the platelet lysates without C10M. Data were quantified by densitometry (Fig. 2C and D).

C10M inhibits pCRP*/mCRP-induced monocyte adhesion and pro-inflammatory cytokine production

pCRP* and mCRP have previously been demonstrated to enhance leukocyte adhesion, transmigration, and subsequent cytokine production, all of which are key events in the inflammatory cascade. Therefore, we next investigated the inhibitory effects of C10M in abrogating these pro-inflammatory properties of CRP. The potential of C10M to inhibit CRP-induced monocyte adhesion, expression of pro-inflammatory cytokines, and formation of platelet-leukocyte aggregates was evaluated *in-vitro*. pCRP*/mCRP was generated by incubation of ADP-stimulated platelets with pCRP as described previously [9,13]. mCRP leads to the formation of platelet-leukocyte aggregates, which can be inhibited by C10M (Fig. 3A - C). In a static monocyte adhesion assay analyzing binding of monocytes to a fibrinogen matrix, pCRP* induces monocyte adhesion, which can be inhibited by C10M (Fig. 3D). Notably, C10M is only reducing the pCRP*-induced exacerbation of inflammation, which is represented by the increase in monocyte adhesion, but not the underlying increase in adhesion of monocytes that is induced by the ADP-activated platelets.

We further analyzed the interaction of platelet-bound pCRP*/mCRP with monocytes by intracellular staining (ICS) and flow cytometry. Cytokine expression levels of pro-inflammatory cytokines, as measured by ICS, were found upregulated in monocytes (Fig. 3E). Tumor necrosis factor (TNF), IL-6 and IL-1β were expressed at a low level when whole blood of healthy donors was incubated for six hours or longer without stimulating agent (control). When incubated with pCRP, expression levels did not differ significantly from control. In contrast, ADP-stimulated platelets cause increased expression of all three cytokines in monocytes, which importantly was significantly increased further by addition of pCRP. These exacerbating effects were blunted by C10M. To confirm the flow cytometric data, we performed confocal fluorescence microscopy (Fig. 3F) and found TNF expression upregulated in cells incubated with ADP-activated platelets and pCRP, resulting in pCRP* formation (middle row). In contrast, cells incubated with activated platelets, pCRP and C10M were not expressing more TNF than the control group (bottom row) due to the inhibition of pCRP* formation (Fig. 3F).

C10M inhibits pCRP binding to activated platelets and microvesicles and reduces pCRP*/mCRP induced ICAM-1 and VCAM-1 expression on human endothelial cells and activation of leukocytes

The interaction of immune cells with activated endothelial cells, leading to cell adhesion and transmigration, is a crucial event in localized tissue inflammation. We investigated the effects of pCRP* on endothelial cells and leukocytes in order to test the therapeutic anti-inflammatory potential of C10M. Circulating pCRP binds to activated cells and is shed on microvesicles largely as pCRP*; this mechanism is crucial in transporting and mediating pCRP* in circulation *in-vivo* [13,27]. We therefore examined the effects of C10M on pCRP binding to human umbilical vein endothelial cell (HUVEC) monolayers and binding of ADP-activated platelets and microvesicles derived from mononuclear cell lines (THP-1) after LPS stimulation. pCRP on platelets and microvesicles, respectively, bind to HUVEC cell monolayers (Figs. 4A, first row and S3A, upper panel). C10M significantly reduces this initial step of pCRP*-mediated aggravation of inflammation (Figs. 4A, second row and S3A, lower panel). In order to test the functional relevance of this process we investigated the expression of ICAM-1 and VCAM-1 in the HUVEC cells. C10M significantly reduces ICAM-1 and VCAM-1 expression induced by pCRP* on platelets and microvesicles, respectively (Figs. 4B, C and S3A). Upregulation of adhesion receptors represents the inflammatory response of the endothelial cells in the initial phase of inflammation [28,29]. ICAM-1 and VCAM-1 are crucial endothelial ligands for receptors of the integrin family, essential for the adhesion and tissue infiltration of leukocytes. In order to look at this mechanism further, we examined the effects of pCRP* on neutrophil (Fig. 4D) and monocyte (Fig. 4E) activation, as determined by CD11b expression [30]. C10M reduces pCRP*-induced monocyte and neutrophil activation (Fig. 4D and E). Generation of reactive oxygen species (ROS) measured by redox-indicator dihydroethidium in flow cytometry served as another pro-inflammatory readout in both monocytes and neutrophils (Fig. S3B). A novel finding of our investigation into the mode of action of CRP-regulated inflammation is that pCRP*/mCRP induces formation of neutrophil extracellular traps (NETs) (Fig. S3C), a process called NETosis. NETosis is a mediator of sterile inflammation, a key event that modulates tissue and organ damage [31]. Our finding

that C10M reduces pCRP*/mCRP-induced NETosis further highlights the relevance of CRP regulation at an important immune checkpoint and the therapeutic potential of C10M.

C10M inhibits CRP-induced aggravation of renal ischemia/reperfusion injury

IRI represents the prototypic sterile inflammation in which an exacerbated immune response leads to unwanted tissue damage. We have previously demonstrated that IRI-associated tissue damage is induced by the pro-inflammatory forms of CRP (pCRP* and mCRP) and that the palindromic inhibitor bis-PC can largely prevent this tissue damage by stabilizing the non-inflammatory pCRP form [8]. Thus, an IRI-induced acute renal injury model in rats represents an ideal *in-vivo* model to evaluate the therapeutic potential of C10M [8]. Firstly, the pharmacokinetic plasma half-life ($t_{1/2}$) of C10M was determined by mass spectrometry to be 90 min in the rat (Fig. 5A and B). C10M is cleared by the kidneys after i.v. administration. After IRI, the rat kidneys were examined for CRP deposits by immunohistochemistry and Western blotting (Fig. 5C and D). Staining for CRP using the conformation-specific anti-pCRP*/mCRP antibody 9C9, which targets an epitope exposed in the pro-inflammatory forms of CRP but not in pCRP [7, 13], demonstrated deposition of the pro-inflammatory forms of CRP specifically localized to the IRI-exposed renal tissue (Fig. 5C). After i.v. administration of C10M, CRP deposition could not be detected in the tissue. This was further confirmed by Western blots of tissue lysates separated by SDS-PAGE (Fig. 5D). The beneficial effects of C10M in IRI was reflected by the significant improvement of excretory renal function as analyzed by blood urea levels (Fig. 5E). To obtain further mechanistic data we assessed the CD68 + monocytic cell infiltration (Fig. 5F) in renal tissue and performed PAS staining of renal tissue (Fig. 5G). In these assays, administration of pCRP leads to significant increase of IRI-associated inflammatory cell infiltration and tissue damage that can be blunted by the administration of C10M.

C10M inhibits pCRP*/mCRP-induced aggravation of allograft rejection in a hindlimb transplantation model

IRI is a major aggravating factor in organ damage and allograft rejection after allograft transplantation [32,33]. To further confirm the therapeutic potential of pCRP*/mCRP inhibition *in-vivo*, we performed hindlimb transplantation on fully mismatched rat strains (Lewis and Brown-Norway) as a model for acute allograft rejection of vascularized composite allografts (VCA) and clinically assessed graft survival (Fig. 6A). We found human pCRP to strongly promote the diapedesis of monocytes and tissue degradation, and thereby to accelerate VCA-graft loss significantly compared to a transplanted control group (control vs pCRP, 7.83 vs 4.83 days; n = 4, each group; *P* value 0.0005, log-rank (Mantel-Cox) test) (Fig. 6B, top, black vs red broken line). Most importantly, premature graft loss driven by pCRP was prevented by i.v. C10M application during the first two days after transplantation (Fig. 6A and B, top, blue broken line). C10M effects are attributable to the inhibition of pCRP* and mCRP, as without extrinsic pCRP application C10M did not show protective effects (Fig. 6B, bottom, blue dotted vs black line).

Transplanted rat hindlimbs showed significant clinical signs of rejection (edema, erythema, and blistering) on day three after transplantation post CRP administration (Fig. 6C) that were not present in the control group or when formation of pCRP*/mCRP was blocked with C10M. Skin and muscle biopsies were taken at day 3 and analyzed histologically. Monocyte infiltration was detected by immunofluorescence microscopy, which revealed significantly more monocyte infiltrates in VCA-tissue of rats treated with pCRP compared to control rats. To investigate whether these exacerbating effects were specific for CRP, C10M was used to block the formation of the pCRP* and mCRP species. In rats treated with both pCRP and C10M, no CRP deposits were detected in either muscle (Fig. 6D) or skin tissue (Fig. 6E). We found the number of transmigrated CD68 + cells to be reduced to control levels when C10M was administered in the pCRP group. Further, we analyzed the amount of depleted CRP in the tissue by Western blotting and found CRP significantly reduced in both muscle and skin (Fig. 6F). These results indicate that compound C10M inhibits the CRP-dependent activation and transmigration and thereby abrogates the CRP-mediated local inflammatory exacerbation in transplant rejection.

C10M does not suppress CRP-independent host defense against pathogens

Phagocytosis of bacteria is a crucial protective mechanism of the innate immune response and CRP-mediated phagocytosis has been previously described [34]. To demonstrate that phagocytosis of *S. pneumoniae* is not abrogated by C10M we performed a flow cytometry-based phagocytosis assay. pCRP leads to a moderate increase in phagocytosis of *S. pneumoniae* in monocytes and neutrophils (Fig. 7A), which is reduced by addition of C10M (Fig. 7B). Baseline phagocytosis is not affected by C10M, suggesting that innate immune mechanisms that have protective functions are not inhibited by C10M.

Material And Methods

Detailed experimental material and methods are described in the Supplementary Information.

Reagents and antibodies

For the biophysical assays and crystallization studies, pCRP was commercially acquired from Merck (Product number: 236608). For the cell assays and animal studies, preparation of human pCRP was performed as described previously by our group [13]. In brief, pCRP purified from human ascites was purchased from Calbiochem (Nottingham, UK) and was thoroughly dialyzed twice (1:500 v/v) against Dulbecco's phosphate buffered saline (DPBS) supplemented with 0.9 mM $CaCl_2$ and 0.49 mM $MgCl_2$. Monomeric CRP (mCRP) was generated by treating pCRP with 8 M urea for 1 hour at 37°C and following dialysis against 25 mM Tris-HCl (pH 8.5) overnight at 4°C as described by Bíro *et al.* [35]. The protein concentration was determined after each dialysis and dissociation procedure by a benchtop fluorometer (Qubit® 3.0 Fluorometer, Invitrogen™ by life technologies™, Carlsbad, CA, USA).

Synthesis of C10M

Synthesis of the compound C10M was achieved using standard synthetic methods (refer to Supplementary Information for full details). Dibutylamine was reacted with diethyl-(3-bromopropyl)phosphonate in dimethylformamide in the presence of a catalytic amount of sodium iodide at elevated temperature. The diethyl protected key intermediate was purified by column chromatography on silica gel and isolated in modest yield (28 %). The diethyl protecting groups on the phosphonate were removed using trimethylsilylbromide in dichloromethane. After removal of the volatiles under vacuum and trituration with hexane, the target material was isolated as the bromide salt in modest yield (44 %) in better than 95% purity as determined by HPLC.

Surface plasmon resonance

A Biacore S200 instrument (GE Healthcare) was used to perform the experiments at 25°C, 30 µl/sec in 10 mM HEPES, 100 mM NaCl, 10 mM $CaCl_2$, 0.005 % Tween pH 7.4 as running buffer. The active flow cell of the CM5 chip (GE Healthcare) was activated using NHS/EDC and the pCRP protein in 50 mM MES pH 6 was immobilized on the chip by amine coupling before blocking with ethanolamine. A range of concentrations of either C10M (0–1600 µM) or PC (0–100 µM) were injected both on the active and reference flow cells. All binding curves were double referenced, with the responses from the blank flow cell and buffer being subtracted from the active cell response during analysis using the S200 Biacore Evaluation software. The RU of each concentration of compound was plotted against the compound concentration to determine the affinity of binding (K_D). The data were expressed as mean ± SEM, each experiment was performed in triplicate.

Crystallization and X-ray crystallography

The pCRP protein was prepared for crystallization by adding 1 µl 100 mM $CaCl_2$ to 50 µl pCRP at 8 mg/ml in 20 mM Tris, 140 mM NaCl, 2 mM $CaCl_2$. Compound C10M was dissolved in water and added to pCRP to achieve a 1:3 molar ratio of pCRP:C10M. Drops of 2 µl size (1:1 volume ratio of well buffer and protein + C10M) were set up over 500 µl reservoir solution at 20 °C in a 24 well Linbro plate using hanging drop vapor diffusion methods. Crystals of pCRP in complex with C10M were obtained with 100 mM Tris pH 9, 10 % PEG 4000, 50 mM LiCl and 200 mM $MgCl_2$ as the well buffer. The crystals were frozen using liquid nitrogen after application of 20% ethylene glycol as cryoprotectant. Diffraction data were collected on the MX2 beamline at the Australian Synchrotron. The structure was solved from the collected dataset by molecular replacement using the previously published structure of the PC:pCRP complex as the input model (PC molecules were removed, PDB ID: 1B09 [24]). The data were processed with XDS [36] and CCP4 [37] followed by refinement using PHENIX [38]. The PDB coordinates have been deposited in the Protein Data Bank under PDB ID: 7L9V.

Human ex-vivo studies

Whole blood and cells isolated from peripheral venous blood used in the assays described hereafter were taken from healthy human volunteers after informed consent. All human studies were approved by the

ethics committee of the University of Freiburg Medical Center (# 112/17) and conducted in accordance with the declaration of Helsinki.

In-vitro and ex-vivo testing of C10M

All cell cultures were tested for mycoplasma contamination on a regular basis. HUVECs were purchased from PromoCell (Heidelberg, Germany) and cultured in supplemented Endothelial Cell Basal Medium (SupplementMix, 10 % FCS, 50 U/ml penicillin, 50 µg/ml streptomycin; PromoCell). The acute monocytic leukemia cell line THP-1 (DKMZ, Braunschweig, Germany) was used for microvesicle preparation and was cultured in RPMI 1640 medium supplemented with 10 % FCS, 2 mM L-glutamine and 50 U/ml penicillin and 50 µg/ml streptomycin. Identity of the utilized cell line was confirmed by *Multiplex Human Cell Line Authentication Test* (Multiplexion, Heidelberg, Germany). Peripheral blood human primary monocytes were isolated from peripheral whole blood using density gradient centrifugation. Blood was taken from normal and healthy volunteers (aged 22–29, male and female) into heparinized tubes (Sarstedt S-Monovette® NH_4 heparin, 16 IU/ml blood). Detailed protocols for *in-vitro* and *ex-vivo* tests performed with C10M are available as online Supplementary Materials and Methods.

Animal experiments

All surgical procedures were conducted according to the recommendations of the animal ethics committee of the University of Freiburg Medical Center, Germany. Both experimental protocols were approved by the animal ethics committee of the University of Freiburg Medical Center, Germany (35-9185.81/G-10/114; 35-9185.81/G-16/53). The renal ischemia/reperfusion-injury (IRI) experiments were carried out on male Wistar rats. All rats were six weeks old and body weight was between 180 and 220 g (Charles River Research Models and Services, Sulzfeld, Germany) as described previously [8]. An acute rejection model of a hindlimb allograft was performed as originally described by Doi [39]. Detailed protocols for the animal experiments are provided as online Supplementary Materials and Methods.

Ischemic acute kidney injury model in rats

The experimental protocol has been described previously by our group [24] and was conducted with minor modifications. In brief, male Wistar rats (six weeks old, body weight 180–220 g) were anesthetized with 1.5–2 vol % isoflurane (Abbott, Wiesbaden, Germany). Both renal pedicles were dissected via two flank incisions and clamped for 45 min followed by a 24 hour reperfusion period. 25 µg pCRP per ml serum volume was injected intraperitoneally at the end of the ischemia and 12 hours later. Rats intravenously received either DPBS (IRI, IRI + pCRP, sham + pCRP) or C10M (IRI + pCRP + C10M, IRI + C10M) in DPBS (1:100 in molar ratio, pCRP to C10M) four times every six hours starting with the beginning of the reperfusion period. After 24 hours, rats were killed and tissue prepared as described previously [24].

Renal excretory function in acute ischemic kidney injury was assessed as described previously [24] by blood urea nitrogen (BUN) concentration in serum. Thus, blood samples were taken at given time points from the tail vein into micro tubes with clotting activator (Micro tube 1.3 ml Z, Clotting Activator/Serum,

Sarstedt) and centrifugated after clotting. BUN was measured using a cobas 8000 modular analyzer (Roche, Basel). Hemolytic samples were discarded.

Immunostaining and histomorphological evaluation

Immunohistochemistry and histomorphological evaluation of the renal tissue was performed on formalin-fixed paraffin-embedded renal tissue sections (5 µm thick serial sections). Paraffin-embedded sections were de-paraffinized in xylol, rehydrated, and boiled for 20 min in concentrated citric acid (pH 6.0). Antigen unmasking for anti-monocyte detection was done by application of pepsin solution (Digest-All™ 3, life technologies) at room temperature for 20 min. Previously, both kidneys were flushed with DPBS followed by fixation in 4 % PFA. Evaluation was performed as described previously [24]: histomorphological changes were evaluated in a blinded fashion by two researchers using a Zeiss microscope (Carl Zeiss Microscopy Axio Imager.M2, Germany) on Periodic acid–Schiff stained sections by quantitative measurement of tubulointerstitial injury, which was assessed by loss of tubular brush border and cast formation. The morphological assessment was scaled in five steps: not present (0), mild (1), moderate (2), severe (3) to very severe (4). Transmigrated leukocytes were detected by anti-rat CD68 antibody (clone ED-1) in a 1:100 dilution and renal inflammation was evaluated by counting ED-1 positive cells in 20 randomized areas of interest of the renal cortex at ×200 magnification. Sections were counterstained with Mayer's hematoxylin. Unspecific isotype matched primary antibodies served as negative control. Detection of human CRP on the renal tissue sections was performed using anti-pCRP*/mCRP antibody 9C9 (1:10 dilution).

Hind limb transplant rejection model

The two inbred stains *Brown-Norway* (BN, recipient) and *Lewis* (LW, donor) show a strong antigenic mismatch [25] and were used for the acute rejection model. The method was first described by Doi [26] and was performed with minor modifications. In brief, two experimenters performed transplantation together: while one is working on the donor rat, another was preparing the recipient rat. In both rats, hind limbs are shaved and thoroughly disinfected, then a circumferential skin incision was performed at mid-thigh level. The donor limb is first fixed by femoral bone osteosynthesis, which was achieved by using an intramedullary rod made from a 0.8 mm *Kirschner* wire. Muscles are then sutured with 4/0 nylon running sutures with adaption of the according functional groups (thigh extensors, adductors, gluteal muscles and hamstrings). This model of acute rejection was set as a non-functional hind limb transplant, so no suturing of the nerves was performed. Revascularization was performed using 9/0 nylon sutures. Both vessels were sutured under the microscope with 8–10 single stiches. The inguinal fat flap (containing the superficial epigastric artery) from the donor hind limb is used to cover the anastomoses to prevent major bleeding. The wounds were rinsed with 0.9 % saline solution and the transplantation is completed by a *Penrose* drain including skin closure with running sutures (4/0 nylon). The skin is cleaned with non-alcoholic disinfectant (Octenisept®, Schülke, Germany) after the skin suture is completed. The total operative time was on average 90 min. All rats received postoperative subcutaneous injections of 100 µg/100 g bodyweight of carprofen for pain relief and 1 ml/100 g bodyweight saline solution for volume

compensation. A plastic collar was used to prevent auto-mutilation and hind limbs with self-inflicted wounds were excluded from further evaluation. For postoperative management after the completion of the skin suture, sufficient reperfusion of the transplanted hind limb was assessed again. Rats then received a first intraperitoneal bolus of 25 µg pCRP per ml serum volume and 500 µl of DPBS supplemented with calcium and magnesium (control), respectively. The second bolus was administered 24 hours after the first. An intravenous catheter (Abbocath-T 26 G, 0.6 x 19 mm) in the tail vein was used to inject C10M (1:100 molar ratio to pCRP) in DPBS and DPBS, respectively, every six hours for the first 42 hours (eight applications in total, starting with the first intraperitoneal bolus) (Fig. 6A). Rats are allowed to awake from anesthesia and cared for until fully awake and warmed. All rats showed slight edema of the transplanted hind limb within the first post-operative day. Rejection of the hind limb graft was assessed by clinical control every 8 hours and graded as described previously [27] according to an established clinical classification for allograft rejection, from 0 (no clinical signs of rejection), 1 (edema), 2 (erythema), and 3 (epidermolysis and desquamation) to 4 (necrosis). Four experimental groups were included in this study (n = 4). In the control group (n = 4, LW◊BN), *Brown-Norway* recipient rats received intraperitoneal DPBS administration. Rats in the pCRP group received two intraperitoneal boli of 25 µg pCRP (BD Micro-Fine™ +Demo, 30G insulin syringes) per ml serum volume directly following to the surgical procedure and after 24 hours. Serum volume was estimated as described previously as a function of the body weight [28]. Immediately after surgery, subcutaneous saline supplementation was given to avoid dehydration of the rats. In the C10M treatment group (n = 4, LW◊BN), rats were treated as in the pCRP group. Additionally, rats received intravenous compound C10M (1:100 molar ratio) via a 26G catheter (Abbocath-T, ICU Medical B.V., Netherlands) in the lateral tail vein every 6 hours for the first two postoperative days. Biopsies were taken on day three after transplantation of skin and muscle tissue and immunohistochemistry performed on formalin-fixed and paraffin embedded samples. After incubation with primary antibody anti-CD68 (clone ED1, 1:100) and anti-human CRP (clone 8, 1:200) for 1 hour at room temperature, slides were incubated with secondary antibody anti-mouse-conjugated CF488 (green) following the manufacturer's protocol.

Pharmacokinetic studies in rats

Plasma concentrations of C10M were measured by an LC-MS method after a single intravenous injection into the tail vein of male Wistar rats (250–350 g). Rats were anesthetized as described above and temperature controlled. 100 µg of C10M was injected and blood samples were taken at given time points (1, 5, 10, 15, 30, 45, 60 and 90 min after bolus injection). EDTA-anticoagulated (1.6 mg/ml EDTA) blood samples were centrifugated for 10 min at 2,000 x g and 4°C to remove the cellular portion. The resulting supernatant was snap frozen and stored at − 80°C until further sample preparation with solid-phase extraction.

Renal excretion of C10M was measured by a model previously described [29] with marginal modifications. Male Wistar rats (300–350 g bodyweight) were anesthetized as described above and the urinary bladder was carefully exposed and externalized under sterile conditions. Sterile urine was drawn from the bladder after a single intravenous application of C10M and C10M + pCRP 15, 30, 45, 60, and 90 min after the i.v.

application, respectively. The urine samples were immediately snap frozen and stored at -80°C until measurements taken. Pharmacokinetic parameters were calculated using PKSolver add-in for Microsoft Excel [30].

SDS-PAGE and Western blotting

For SDS-PAGE, tissue lysates from rat kidneys, muscle and skin tissue samples were precipitated on ice with same volumes of 10 % trichloroacetic acid after homogenization with a disperser tool on ice (Ultra Turrax® IKA®, Germany). Pelleted protein was denaturated in SDS loading dye supplemented with DTT at 95°C, 5 min and then separated on 10–12 % SDS-polyacrylamide gels. After Western blot, nitrocellulose membranes were blocked in 5 % BSA in TBS-T and incubated with mouse anti-human CRP antibody (Clone CRP-8, 1:2,000). HRP-conjugated goat anti-mouse antibody 1:5,000 v/v in 1 % BSA-TBS-T was used to detected bound CRP antibodies after washing steps. GAPDH served as loading control and was detected with anti-human GAPDH-HRP (1:1,000 in 1 % BSA in TBS-T). Protein bands were visualized using ECL™ Western blotting analysis system (GE Healthcare, United Kingdom), medical x-ray film (Fujifilm, Japan), and developed on a CURIX 60 developer (AGFA).

For detection of CRP in IRI kidneys, snap frozen tissue was homogenized on ice using a high-power disperser in lysis buffer with added protease inhibitors. After centrifugation of the homogenized tissue, the supernatant was transferred, and protein concentrations were determined with BCA protein assay, and processed as described above.

For semiquantitative analysis of CRP binding to activated human platelets, we performed SDS-PAGE and Western blotting as described previously [10]. Briefly, human platelets were isolated and washed from citrate-anticoagulated whole blood by differential centrifugation in sequestrene buffer. pCRP (100 µg/ml) was incubated with ADP-activated platelets and C10M at different concentrations (10 mM and 100 mM, Fig. 2C showing 10 mM). Calcium-depleted platelets served as a control. Platelets were then washed three times in DPBS supplemented with calcium. Platelets were pelleted, resuspended in 10 mM HEPES buffer at pH 7.4, 10 mM KCl, 1.5 mM $MgCl_2$, 1 mM EDTA, with added protease inhibitors (10 µl of 200 mM PMSF in DMSO, protease inhibitor cocktail in DMSO, 100 mM Na-orthovanadate per 1 ml) (sc24948 RIPA Lysis Buffer System, Santa Cruz, Biotechnology, Dallas, TX, USA) and homogenized on ice by applying shear-stress followed by freeze-and-thaw cycles in liquid nitrogen. The protein concentration of the lysates was determined by fluorometric assay using a Qubit fluorometer. After the separation by SDS gel electrophoresis and the transfer to nitrocellulose membranes (Hybond ECL, GE Healthcare, Munich, Germany), samples were probed with anti-CRP antibody clone 8 overnight at 4°C. Monoclonal antibodies against GAPDH (abcam, Cambridge, UK) were used to ensure protein equilibration. Secondary HRP-conjugated anti-mouse antibodies (Dianova, Hamburg, Germany), enhanced chemiluminescence (ECL, GE Healthcare) were used to detect protein signals and were conserved on FUJI Medical X-Ray Film (FUJIFILM, Japan).

Statistical analyses

All statistical analyses were performed using GraphPad Prism v9.0 for Mac (GraphPad Software, La Jolla, California, USA). Experiments were performed at least three times. The data are shown as mean and standard error of the mean (SEM) as indicated. One-way analysis of variance (ANOVA) and post-hoc *Tukey's* test was used to compare more than two groups. If only two groups were compared, a two-tailed *Student's* t-test was employed. A *P* value of < 0.05 was considered statistically significant.

Discussion

C-reactive protein is an evolutionary highly conserved and central player in inflammatory diseases [1]. The circulating isoform of CRP, pCRP, binds to PC and PE head groups of bioactive lipids exposed on the membranes of damaged cells and microvesicles, which subsequently leads to the formation of the pro-inflammatory CRP isoforms, pCRP* and mCRP [3,12]. This CRP 'activating' mechanism has only recently been identified [3,9,11,13]. It transforms a relatively inert molecule, pCRP, to highly pro-inflammatory molecules, pCRP* and mCRP, both contributing to and aggravating tissue damage [8,11,12]. Disrupting the interaction between pCRP and PC/PE, and thereby inhibiting this 'CRP activation', represents a novel and attractive anti-inflammatory strategy. Targeting the direct interaction between PC/PE and pCRP, we employed a combination of medicinal chemistry and computational modeling to develop a novel low molecular weight inhibitor that binds to the PC/PE binding pocket of pCRP thereby blocking pCRP binding to exposed PC/PE head groups and consequently blocking 'CRP activation'. Utilizing SPR and X-ray crystallography as direct protein binding assays, in combination with *in-vitro* binding assays, we demonstrate that the small molecule, C10M, binds to the PC/PE binding pocket of pCRP in a competitive manner. C10M inhibits pCRP*/mCRP-induced monocyte adhesion, cytokine and ROS production, NET formation as well as pCRP*/mCRP-mediated upregulation of endothelial ICAM-1 and VCAM-1. Most importantly, C10M affords significant protection from CRP-mediated tissue injury in two distinct pre-clinical models of inflammation, a model of renal IRI and hindlimb transplantation.

Our approach contrasts to the previously described mode of action for bis-PC, a compound that combines two PC moieties into one bivalent molecule. Bis-PC prevents the formation of pCRP* and mCRP by each of its PC portions binding to the PC/PE binding pocket on two separate pCRP molecules, thereby bringing the two pentamers together with opposing B-faces in a doughnut-like decameric arrangement [5]. Within this decamer structure, the pCRP B-faces are no longer available to bind to exposed PC/PE head groups of bioactive lipids and the 'CRP activation' step is blocked [5]. It had been suggested that the CRP-inhibitory effect of bis-PC was primarily due to its bivalency (i.e., two functional PC head groups), however we hypothesized that a compound with just one head group would be able to elicit an anti-inflammatory response. Here, we explored this hypothesis by designing a low molecular weight (~ 250 Da) molecule, C10M, which mimics PC by binding to the PC/PE binding pocket on pCRP, thereby stabilizing the inert, non-inflammatory form of CRP by competitively inhibiting the binding of pCRP to exposed PC/PE head groups of bioactive lipids. The binding mode of C10M to pCRP was confirmed by X-ray crystallography, showing that the phosphonate moiety was the main anchor point of the compound to pCRP. The mode of action of C10M was further investigated and the therapeutic potential of C10M is

supported by our following findings (as summarized in the schematic drawing depicted in Fig. 8): (1) Biophysical assays and X-ray crystallography reveal a specific, stable and competitive binding of C10M to the PC/PE binding pocket of pCRP. (2) C10M binds pCRP and prevents pCRP binding to activated/damaged cell membranes. (3) In turn, this prevents the conformational change from pCRP to pCRP*/mCRP and their tissue deposition in the area of inflammation. (4) C10M is therefore inhibiting the exacerbation of inflammation by CRP, rather than being a general anti-inflammatory drug. (5) C10M reduces tissue damage in a renal IRI model and reduces CRP-mediated acceleration of allograft rejection. (6) C10M does not inhibit CRP-independent phagocytosis suggesting that protective innate immune properties remain intact.

pCRP binding to membrane phospholipids of apoptotic cells has been described previously [40,41]. The phospholipase A2-dependent membrane changes in apoptosis and cell activation that lead to the generation of LPC appear to be crucial in mediating pCRP binding to cell membranes, as pCRP neither binds to non-activated leukocytes [13] nor the ubiquitous PC head groups in the plasma membrane of healthy living cells. We recently showed that the membrane curvature of healthy cells prevents access to the PC/PE binding pocket of pCRP [13]. Once cell membranes are damaged, the membrane curvature increases, as is the case in microvesicles that avidly bind and transport pCRP*/mCRP [13,27]. Therefore, we chose the PC/PE binding pocket of pCRP as the target for our drug discovery approach. As PC/PE head groups are only accessible for pCRP binding after an inflammatory stimulus or in apoptosis, this therapeutic targeting concept aims at the inhibition of the binding events critical to the generation of ‘activated’ CRP to minimize any side effects compared to general pCRP inhibition and reduction of circulating pCRP levels such as achievable by anti-sense oligonucleotides [21] or by CRP-apheresis via binding to a PC resin [22]. This was considered crucial in our inhibitor design, as inflammation can clearly be beneficial as a defense and repair mechanism of the organism. Thus, anti-inflammatory strategies are often considered “two-edged swords” as most anti-inflammatory therapies come at the cost of some level of immune suppression which can lead to significant side effects. Moreover, a small molecule inhibitor is likely to offer significant advantages compared to either anti-sense oligonucleotides or CRP-apheresis given the potential ability to administer small molecule inhibitors via the oral or parenteral route, in addition to having an immediate onset. In contrast, the use of anti-sense oligonucleotides to inhibit CRP expression requires pre-treatment over weeks making this approach unsuitable for acute applications such as IRI. Whilst CRP-apheresis is effective at depleting CRP acutely and thus highly attractive in the acute/emergency setting of tertiary hospitals, the use of apheresis is time consuming and contingent upon the availability of the necessary infrastructure. Therefore, a small molecule CRP inhibitor is highly desirable given the potential ease of administration and suitability for acute and chronic indications.

It is important to emphasize that we adopted an approach that provides a selective therapeutic strategy, only inhibiting the uncontrolled exacerbation of inflammation by pCRP*/mCRP but not inflammation *per se*. We confirm this in our *in-vitro* monocyte assays, in which we analyze the mode of action of our compound. In these assays we use pCRP*/mCRP on the surface of ADP-stimulated platelets to stimulate monocyte adhesion and cytokine expression. Our data confirms our hypothesis that C10M is inhibiting

the effects caused by pCRP*/mCRP, but not the increase in inflammation that is induced by ADP-stimulated platelets, by stabilizing the non-inflammatory pCRP species. Further supporting the concept that the basic innate immune response is not affected by C10M, we demonstrate that phagocytosis is not inhibited by C10M. Indeed, neutrophil phagocytosis and killing of bacteria are essential for host defense against bacteria such as pneumococci [42] and pCRP mediates an increased resistance to bacterial infections [43] via binding to bacterial PC and opsonization of bacteria [44]. We demonstrate that C10M does not inhibit phagocytosis of *S. pneumonia*, zymosan or *E. coli* by monocytes and neutrophils, suggesting that the protective capacities of these innate immune cells are maintained. This is crucial for an anti-inflammatory treatment with reduced side effects. These are important observations since a major aim of our therapeutic approach is to target the uncontrolled exacerbation of inflammation rather than inflammation or innate immunity in general.

To validate the effect of C10M *in-vivo*, we used two distinct animal models of inflammation. Firstly, an established renal IRI model [8] in which we previously demonstrated that pCRP*/mCRP lead to enhanced leukocyte activation, tissue infiltration and generation of ROS resulting in aggravation of tissue injury [8]. This is an ideal model to investigate the anti-inflammatory properties of C10M as IRI represents the prototypic, sterile inflammatory setting that results in increased tissue damage. Secondly, the relevance of IRI for allograft survival after tissue transplantation was investigated. The initial inflammatory stage after transplantation is characterized by IRI and has a crucial impact on long term allograft survival. Indeed, the infiltration of kidney allografts by macrophages within 10 days of transplantation is associated with worse clinical outcome [45,46]. Furthermore, episodes of acute allograft rejection in the first post-transplantation period have a severe negative impact on long-term allograft survival [47]. Therefore, we used a well described allograft rejection model (hindlimb transplantation as a model of vascularized composite tissue allotransplantation – VCA) [48] to test the therapeutic potential of C10M. We demonstrate that CRP accelerates allograft rejection via aggravation of IRI and activation of the innate immune response. In both animal models, we establish C10M's unique benefits in reducing CRP-mediated tissue damage. In the VCA model the acceleration of acute allograft rejection by CRP is reversed by administration of C10M. In the IRI model, renal function is significantly improved and histological signs of kidney injury are markedly reduced. The deposition of CRP in the tissue of renal IRI is significantly reduced after administration of C10M, confirming our *in-vitro* findings that pCRP binding to activated cell membranes, which we have demonstrated to be a prerequisite for subsequent tissue deposition in the area of inflammation, is reduced [11]. For our *in-vivo* experiments we utilized rat models, as although rats have abundant pCRP (300–600 µg/ml in normal healthy pathogen-free rats), rat CRP is not utilized as an acute phase protein and rat complement is not activated by rat CRP [49]. This is in contrast to human CRP that activates both rat and human complement, but not mouse complement [50]. Therefore, rats supplemented with human pCRP are a suitable animal model for CRP research [8,10].

In our experiments, intermittent C10M i.v. injections were sufficient to obtain protective effects in two animal models of localized inflammation. The development of C10M as a novel small molecule inhibitor of CRP provides important proof of concept that such a therapeutic strategy holds significant promise as

a targeted anti-inflammatory approach and paves the way for future compound design, potentially further optimizing pharmaceutical properties. In conclusion, competitively blocking the PC/PE binding pocket on pCRP with C10M is a successful and attractive strategy to reduce CRP-mediated aggravation of inflammation. Significantly, given the wide range of clinical conditions where CRP-mediated tissue damage has been demonstrated, the therapeutic targeting of CRP with small molecule inhibitors is likely to be of broad clinical relevance and can potentially be used in many inflammatory diseases.

Acknowledgements

This work was supported by personal grants to SUE from the German Research Foundation (DFG) EI 866/1-1, EI 866/1-2 and EI 866/10-1 and by a seed grant from the Baker Department of Cardiometabolic Health, University of Melbourne. This research was partly undertaken at the Australian Synchrotron, part of the Australian Nuclear Science and Technology Organization, and made use of the ACRF Detector on the MX2 beamline. We thank the beamline staff for their assistance. Funding from the Victorian Government Operational Infrastructure Support Scheme to St Vincent's Institute and the Baker Institute is acknowledged. JDM is a National Heart Foundation Fellow. JDM, MWP and KP are National Health and Medical Research Council (NHMRC) of Australia Research Fellows. SUE is a Heisenberg Professor of the DFG (EI 866/9-1). Laser scanning microscopy equipment was provided by the DFG as an institutional grant (INST 39/1137-1FUGG).

References

1 McFadyen, J. D. *et al.* C-Reactive Protein and Its Structural Isoforms: An Evolutionary Conserved Marker and Central Player in Inflammatory Diseases and Beyond. *Subcell Biochem* **94**, 499-520, doi:10.1007/978-3-030-41769-7_20 (2020).

2 Lane, T. *et al.* Infusion of pharmaceutical-grade natural human C-reactive protein is not proinflammatory in healthy adult human volunteers. *Circ Res* **114**, 672-676, doi:10.1161/CIRCRESAHA.114.302770 (2014).

3 McFadyen, J. D. *et al.* Dissociation of C-Reactive Protein Localizes and Amplifies Inflammation: Evidence for a Direct Biological Role of C-Reactive Protein and Its Conformational Changes. *Front Immunol* **9**, 1351, doi:10.3389/fimmu.2018.01351 (2018).

4 Griselli, M. *et al.* C-reactive protein and complement are important mediators of tissue damage in acute myocardial infarction. *J Exp Med* **190**, 1733-1740 (1999).

5 Pepys, M. B. *et al.* Targeting C-reactive protein for the treatment of cardiovascular disease. *Nature* **440**, 1217-1221 (2006).

6 Gill, R., Kemp, J. A., Sabin, C. & Pepys, M. B. Human C-reactive protein increases cerebral infarct size after middle cerebral artery occlusion in adult rats. *J Cereb Blood Flow Metab* **24**, 1214-1218,

doi:00004647-200411000-00003 [pii] (2004).

7 Padilla, N. D. *et al.* C-reactive protein and natural IgM antibodies are activators of complement in a rat model of intestinal ischemia and reperfusion. *Surgery* **142**, 722-733, doi:S0039-6060(07)00356-X [pii]

10.1016/j.surg.2007.05.015 (2007).

8 Thiele, J. R. *et al.* A Conformational Change in C-Reactive Protein Enhances Leukocyte Recruitment and Reactive Oxygen Species Generation in Ischemia/Reperfusion Injury. *Front Immunol* **9**, 675, doi:10.3389/fimmu.2018.00675 (2018).

9 Eisenhardt, S. U. *et al.* Dissociation of pentameric to monomeric C-reactive protein on activated platelets localizes inflammation to atherosclerotic plaques. *Circ Res* **105**, 128-137, doi:10.1161/CIRCRESAHA.108.190611 (2009).

10 Braig, D. *et al.* A conformational change of C-reactive protein in burn wounds unmasks its proinflammatory properties. *Int Immunol*, doi:10.1093/intimm/dxu056 (2014).

11 Thiele, J. R. *et al.* Dissociation of pentameric to monomeric C-reactive protein localizes and aggravates inflammation: in vivo proof of a powerful proinflammatory mechanism and a new anti-inflammatory strategy. *Circulation* **130**, 35-50, doi:10.1161/CIRCULATIONAHA.113.007124 (2014).

12 Molins, B., Pena, E., de la Torre, R. & Badimon, L. Monomeric CRP is prothrombotic and dissociates from circulating pentameric CRP on adhered activated platelets under flow. *Cardiovasc Res*, doi:cvr226 [pii] 10.1093/cvr/cvr226 (2011).

13 Braig, D. *et al.* Transitional changes in the CRP structure lead to the exposure of proinflammatory binding sites. *Nature communications* **8**, 14188, doi:10.1038/ncomms14188 (2017).

14 Khreiss, T., Jozsef, L., Potempa, L. A. & Filep, J. G. Loss of pentameric symmetry in C-reactive protein induces interleukin-8 secretion through peroxynitrite signaling in human neutrophils. *Circ Res* **97**, 690-697 (2005).

15 Khreiss, T., Jozsef, L., Potempa, L. A. & Filep, J. G. Conformational rearrangement in C-reactive protein is required for proinflammatory actions on human endothelial cells. *Circulation* **109**, 2016-2022 (2004).

16 Zouki, C., Haas, B., Chan, J. S., Potempa, L. A. & Filep, J. G. Loss of pentameric symmetry of C-reactive protein is associated with promotion of neutrophil-endothelial cell adhesion. *J Immunol* **167**, 5355-5361 (2001).

17 Khreiss, T. *et al.* Loss of pentameric symmetry of C-reactive protein is associated with delayed apoptosis of human neutrophils. *J Biol Chem* **277**, 40775-40781 (2002).

18 Tegler, L. T. *et al.* Powerful protein binders from designed polypeptides and small organic molecules–a general concept for protein recognition. *Angew Chem Int Ed Engl* **50**, 1823-1827, doi:10.1002/anie.201005059 (2011).

19 Kumaresan, P. R. *et al.* Synthesis and characterization of a novel inhibitor of C-reactive protein-mediated proinflammatory effects. *Metab Syndr Relat Disord* **11**, 177-184, doi:10.1089/met.2012.0123 (2013).

20 Warren, M. & Flaim, J. D. Modulation of Inflammatory Responses by C-reactive Protein *International Patent* **WO 2104160211** (2014).

21 Warren, M. S., Hughes, S. G., Singleton, W., Yamashita, M. & Genovese, M. C. Results of a proof of concept, double-blind, randomized trial of a second generation antisense oligonucleotide targeting high-sensitivity C-reactive protein (hs-CRP) in rheumatoid arthritis. *Arthritis Res Ther* **17**, 80, doi:10.1186/s13075-015-0578-5 (2015).

22 Ries, W., Heigl, F., Garlichs, C., Sheriff, A. & Torzewski, J. Selective C-Reactive Protein-Apheresis in Patients. *Ther Apher Dial* **23**, 570-574, doi:10.1111/1744-9987.12804 (2019).

23 Christopeit, T., Gossas, T. & Danielson, U. H. Characterization of Ca2+ and phosphocholine interactions with C-reactive protein using a surface plasmon resonance biosensor. *Anal Biochem* **391**, 39-44, doi:10.1016/j.ab.2009.04.037 (2009).

24 Thompson, D., Pepys, M. B. & Wood, S. P. The physiological structure of human C-reactive protein and its complex with phosphocholine. *Structure* **7**, 169-177 (1999).

25 Diehl, P. *et al.* Lysophosphatidylcholine is a Major Component of Platelet Microvesicles Promoting Platelet Activation and Reporting Atherosclerotic Plaque Instability. *Thromb Haemost* **119**, 1295-1310, doi:10.1055/s-0039-1683409 (2019).

26 Eisenhardt, S. U., Habersberger, J. & Peter, K. Monomeric C-reactive protein generation on activated platelets: the missing link between inflammation and atherothrombotic risk. *Trends Cardiovasc Med* **19**, 232-237, doi:10.1016/j.tcm.2010.02.002

S1050-1738(10)00004-6 [pii] (2009).

27 Habersberger, J. *et al.* Circulating microparticles generate and transport monomeric C-reactive protein in patients with myocardial infarction. *Cardiovasc Res* **96**, 64-72, doi:10.1093/cvr/cvs237

cvs237 [pii] (2012).

28 Rothlein, R., Dustin, M. L., Marlin, S. D. & Springer, T. A. A human intercellular adhesion molecule (ICAM-1) distinct from LFA-1. *J Immunol* **137**, 1270-1274 (1986).

29 Yang, L. *et al.* ICAM-1 regulates neutrophil adhesion and transcellular migration of TNF-alpha-activated vascular endothelium under flow. *Blood* **106**, 584-592, doi:10.1182/blood-2004-12-4942 (2005).

30 Eisenhardt, S. U. *et al.* Generation of activation-specific human anti-alphaMbeta2 single-chain antibodies as potential diagnostic tools and therapeutic agents. *Blood* **109**, 3521-3528, doi:blood-2006-03-007179 [pii]

10.1182/blood-2006-03-007179 (2007).

31 Cahilog, Z. *et al.* The Role of Neutrophil NETosis in Organ Injury: Novel Inflammatory Cell Death Mechanisms. *Inflammation* **43**, 2021-2032, doi:10.1007/s10753-020-01294-x (2020).

32 Dashkevich, A. *et al.* Ischemia-Reperfusion Injury Enhances Lymphatic Endothelial VEGFR3 and Rejection in Cardiac Allografts. *Am J Transplant* **16**, 1160-1172, doi:10.1111/ajt.13564 (2016).

33 Nieuwenhuijs-Moeke, G. J. *et al.* Ischemia and Reperfusion Injury in Kidney Transplantation: Relevant Mechanisms in Injury and Repair. *J Clin Med* **9**, doi:10.3390/jcm9010253 (2020).

34 Mold, C., Gresham, H. D. & Du Clos, T. W. Serum amyloid P component and C-reactive protein mediate phagocytosis through murine Fc gamma Rs. *J Immunol* **166**, 1200-1205 (2001).

35 Biro, A. *et al.* Studies on the interactions between C-reactive protein and complement proteins. *Immunology* **121**, 40-50, doi:IMM2535 [pii]

10.1111/j.1365-2567.2007.02535.x (2007).

36 Kabsch, W. Integration, scaling, space-group assignment and post-refinement. *Acta Crystallographica Section D Biolgical Crystallography* **66**, 133-144, doi:10.1107/S0907444909047374 (2010).

37 McCoy, A. J. *et al.* Phaser crystallographic software. *J Appl Crystallogr* **40**, 658-674, doi:10.1107/S0021889807021206 (2007).

38 Adams, P. D. *et al.* PHENIX: a comprehensive Python-based system for macromolecular structure solution. *Acta Crystallogr D Biol Crystallogr* **66**, 213-221, doi:10.1107/S0907444909052925 (2010).

39 Doi, K. Homotransplantation of limbs in rats. A preliminary report on an experimental study with nonspecific immunosuppressive drugs. *Plastic and reconstructive surgery* **64**, 613-621 (1979).

40 Chang, M. K., Binder, C. J., Torzewski, M. & Witztum, J. L. C-reactive protein binds to both oxidized LDL and apoptotic cells through recognition of a common ligand: Phosphorylcholine of oxidized phospholipids. *Proc Natl Acad Sci U S A* **99**, 13043-13048 (2002).

41 Gershov, D., Kim, S., Brot, N. & Elkon, K. B. C-Reactive protein binds to apoptotic cells, protects the cells from assembly of the terminal complement components, and sustains an antiinflammatory innate

immune response: implications for systemic autoimmunity. *J Exp Med* **192**, 1353-1364, doi:10.1084/jem.192.9.1353 (2000).

42 Agrawal, A., Suresh, M. V., Singh, S. K. & Ferguson, D. A., Jr. The protective function of human C-reactive protein in mouse models of Streptococcus pneumoniae infection. *Endocr Metab Immune Disord Drug Targets* **8**, 231-237, doi:10.2174/187153008786848321 (2008).

43 Simons, J. P. *et al.* C-reactive protein is essential for innate resistance to pneumococcal infection. *Immunology* **142**, 414-420, doi:10.1111/imm.12266 (2014).

44 Mukerji, R. *et al.* Pneumococcal surface protein A inhibits complement deposition on the pneumococcal surface by competing with the binding of C-reactive protein to cell-surface phosphocholine. *J Immunol* **189**, 5327-5335, doi:10.4049/jimmunol.1201967 (2012).

45 McLean, A. G. *et al.* Patterns of graft infiltration and cytokine gene expression during the first 10 days of kidney transplantation. *Transplantation* **63**, 374-380 (1997).

46 Raftery, M. J. *et al.* The relevance of induced class II HLA antigens and macrophage infiltration in early renal allograft biopsies. *Transplantation* **48**, 238-243 (1989).

47 Matas, A. J., Gillingham, K. J., Payne, W. D. & Najarian, J. S. The impact of an acute rejection episode on long-term renal allograft survival (t1/2). *Transplantation* **57**, 857-859 (1994).

48 Radu, C. A. *et al.* Mitomycin-C-treated peripheral blood mononuclear cells (PBMCs) prolong allograft survival in composite tissue allotransplantation. *J Surg Res* **176**, e95-e101, doi:10.1016/j.jss.2011.12.032 (2012).

49 de Beer, F. C. *et al.* Isolation and characterization of C-reactive protein and serum amyloid P component in the rat. *Immunology* **45**, 55-70 (1982).

50 Reifenberg, K. *et al.* Role of C-reactive protein in atherogenesis: can the apolipoprotein E knockout mouse provide the answer? *Arterioscler Thromb Vasc Biol* **25**, 1641-1646 (2005).

51 Kiefer, J. *et al.* An Unbiased Flow Cytometry-Based Approach to Assess Subset-Specific Circulating Monocyte Activation and Cytokine Profile in Whole Blood. *Front Immunol* **12**, 641224, doi:10.3389/fimmu.2021.641224 (2021).

52 Megyesi, J., Andrade, L., Vieira, J. M., Jr., Safirstein, R. L. & Price, P. M. Positive effect of the induction of p21WAF1/CIP1 on the course of ischemic acute renal failure. *Kidney Int* **60**, 2164-2172, doi:10.1046/j.1523-1755.2001.00044.x (2001).

53 Megyesi, J., Safirstein, R. L. & Price, P. M. Induction of p21WAF1/CIP1/SDI1 in kidney tubule cells affects the course of cisplatin-induced acute renal failure. *J Clin Invest* **101**, 777-782, doi:10.1172/JCI1497 (1998).

Figures

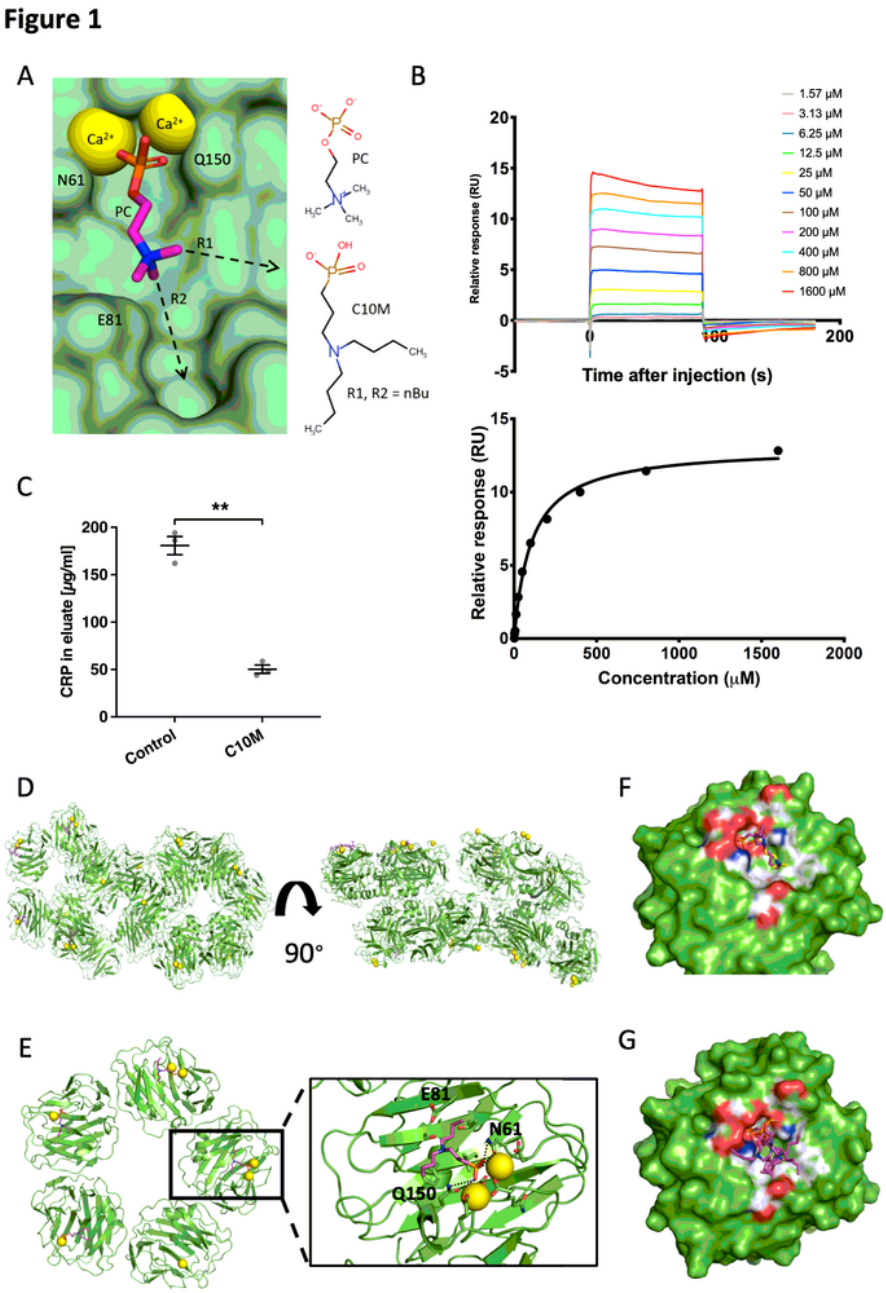

Figure 1

Compound C10M binds to pCRP in-vitro. (A) Design of the phosphonate compound C10M was guided by the PC:pCRP complex (PDB ID: 1B09) 24, with two n-butyl substituents (nBu) on the tertiary amine exploiting available space in the binding pocket along the denoted vectors R1 and R2. Ca2+ cations

shown as yellow spheres and the location of pCRP residues Asn 61 (N61), Glu 81 (E81) and Gln 150 (Q150) are indicated. pCRP depicted as a light green molecular surface. (B) The binding affinity (KD) for C10M to captured pCRP was determined by SPR as 105 ± 12 μM (n = 3). (C) C10M reduces binding of pCRP to immobilized PC. 200 μg pCRP was incubated with p-aminophenyl phosphoryl choline agarose beads under binding conditions with and without C10M (43.5 μg/ml). Porous solid column chromatography was then used to evaluate the binding capacity of pCRP to PC. Protein concentration in eluates was measured with a fluorometric protein assay. n = 3, mean ± SEM. P value was calculated with Student's t-test. **P <0.01. (D) The crystal structure of pCRP (shown as cartoon) in complex with C10M (colored sticks) confirmed that the compound binds to the same pocket as PC/PE. The asymmetric unit consisted of 4 stacked pCRP pentamers. C10M was bound to five CRP monomeric subunits, four in one pentamer and one in another (Table S1). Ca2+ cations depicted as yellow spheres. (E) Structure of the pentamer containing four C10M molecules. Interaction of the phosphonate moiety with the bound Ca2+ cations (yellow spheres) anchors the compound in the binding pocket. A zoom in view of one CRP monomer is shown in the right-hand panel, a full list of interacting residues is given in Table S1. (F) Alignment of C10M (pink/blue/red/yellow sticks) and PC (yellow/blue/red sticks) in complex with pCRP (this work and PDB ID: 1B09 24) via the Cα atoms of pCRP. One monomeric subunit of pCRP is depicted as a molecular surface, the location of acidic (red), basic (blue) and hydrophobic (grey) residues around the PC binding pocket is indicated. Ca2+ cations not shown for clarity. (G) Alignment of the five pCRP monomeric subunits bound to C10M in the asymmetric unit via the Cα atoms of pCRP, illustrating the conformational flexibility of the C10M compound. C10M is anchored into the binding pocket by the interaction of the phosphonate moiety with the bound Ca2+ cations. Ca2+ cations not shown for clarity.

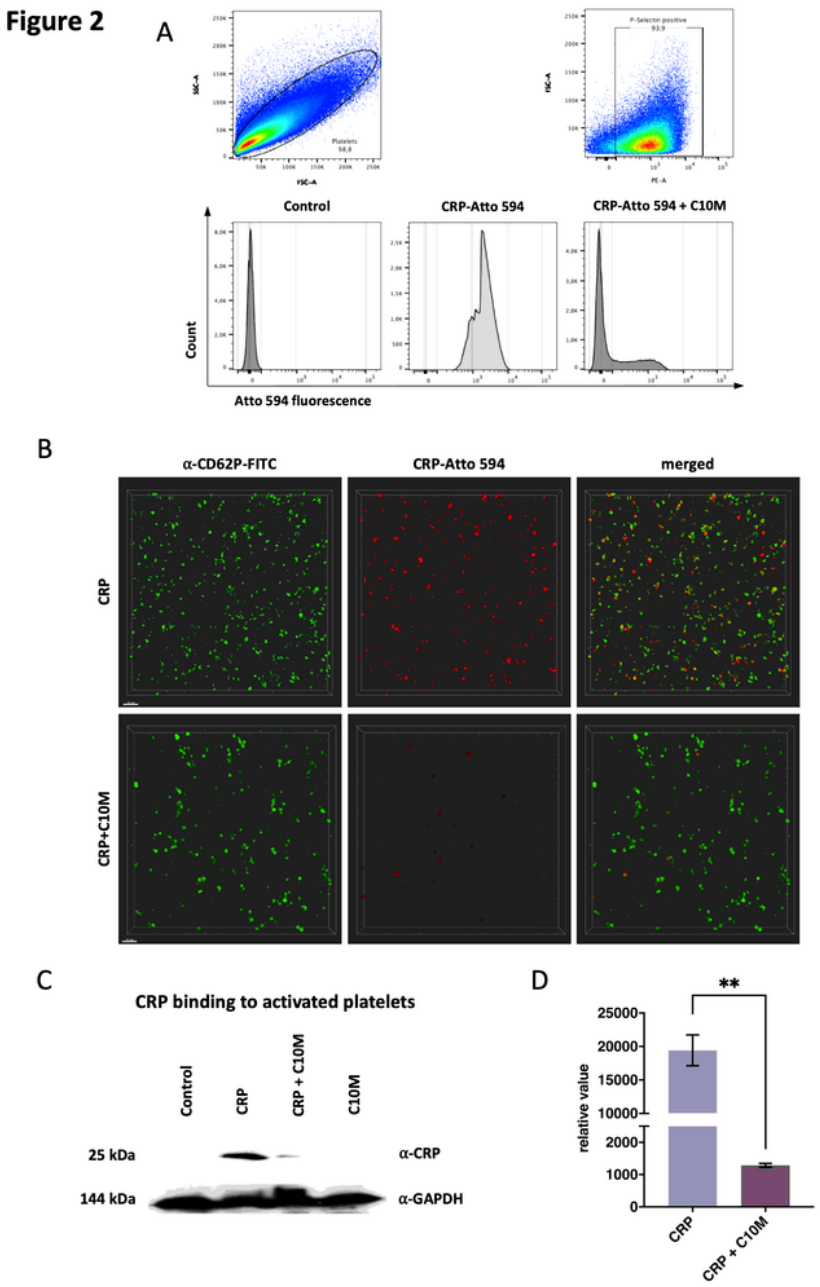

Figure 2

C10M prevents pCRP binding to activated platelets. (A) Flow cytometry was used to determine binding of pCRP-Atto594 to ADP-activated platelets. P-selectin positive platelets were gated using an anti-CD62P-PE antibody and Atto594 fluorescence was analyzed, comparing control without CRP, labeled CRP (50 µg/ml) without and with C10M (43 µM). (B) Confocal fluorescence microscopy of ADP-activated human platelets in the presence of pCRP. Depicted are 3D reconstructions of monolayers of ADP (20 µM)

activated platelets. Platelets were isolated, washed and stained (anti-CD62P FITC, green) from 3.8 % sodium-citrated human whole blood. 50 µg/ml pCRP-Atto594 (red) was incubated with isolated platelets (green) with (bottom) or without (top) C10M in a 1:100 molar ratio. pCRP localizes on the plasma membrane, which can be inhibited by C10M. Scale bar: 20 µm. (C) Western blot of CRP binding to activated platelets. Platelets bind less CRP when incubated with C10M as detected with the anti-CRP antibody (clone CRP-8), compared to the anti-GAPDH antibody (clone 0411) as a control. Washed platelets isolated from human citrated whole blood were incubated with pCRP and C10M, respectively, lysed and separated on SDS-PAGE. (D) Densitometric quantification of protein bands of Western blots (n = 3) from the experiment described in (C) using ImageJ. P value was calculated by Student's t-test. **P <0.01.

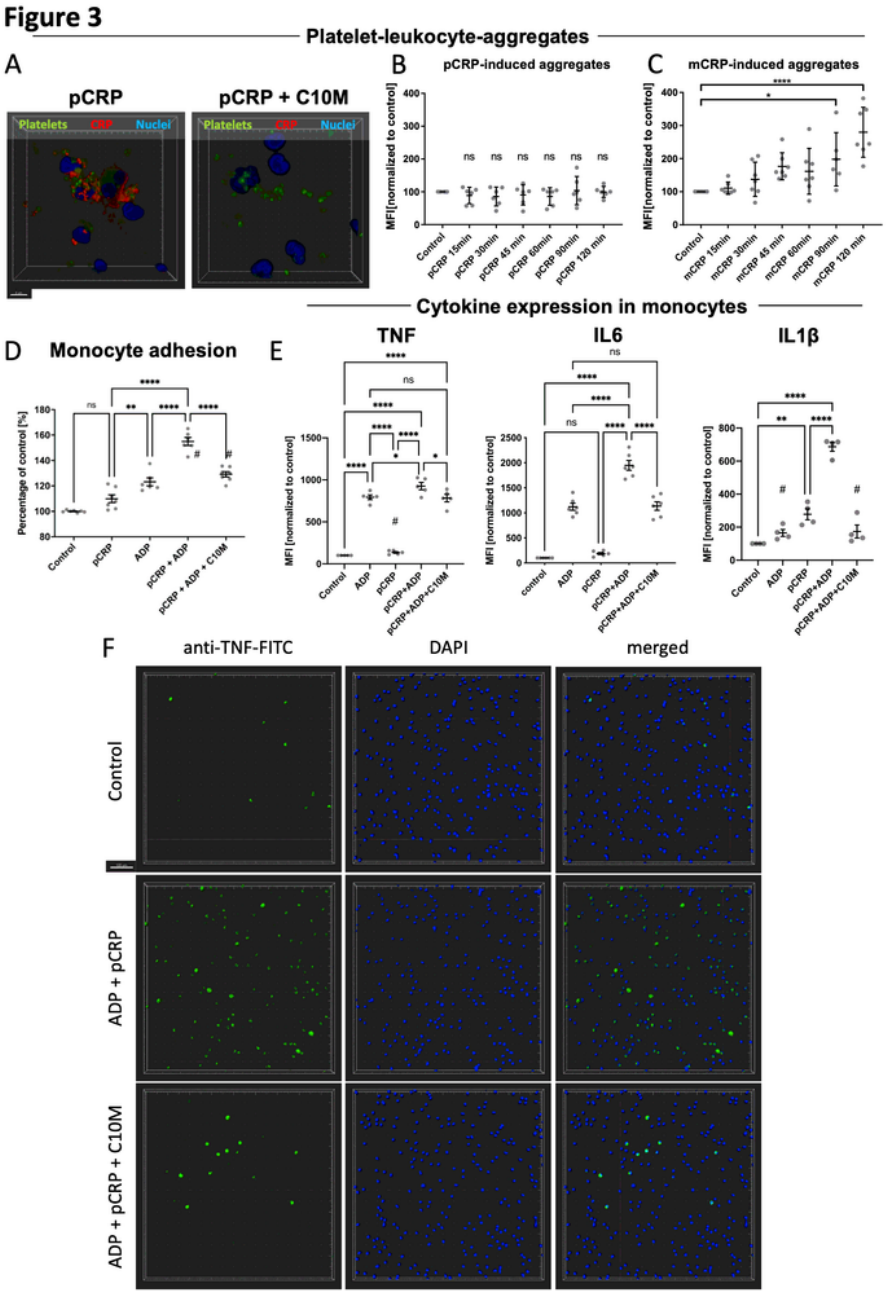

Figure 3

CRP-dependent expression of pro-inflammatory cytokines is abolished by C10M. (A) CRP-coated platelets visualized by fluorescence confocal microscopy bound to whole blood leukocytes. Washed platelets stained with calcein (green) were incubated in serum supplemented with 50 µg/ml pCRP-Atto594 (red), without (left) and with C10M (right) (10.75 µg/ml). Platelets were then added to whole blood samples and imaged after RBC lysis. Shown are platelet-leukocyte-aggregates with and without CRP attached. (B,

C) CRP induces platelet-leukocyte aggregation in a time-dependent and conformation-specific manner. Whole blood samples stimulated with either 50 µg/ml pCRP or mCRP were analyzed by flow cytometry. Double positive events (CD62P and CD14) were identified as platelet-monocyte complexes. Incubation was stopped at indicated time points. Displayed are mean ± SEM. P values were calculated with ANOVA and Tukey's post hoc test. n = 6, *P <0.05, ****P <0.0001, ns: not significant. (D) Static adhesion of monocytes to 20 µg/ml fibrinogen in PBS supplemented with calcium and magnesium was tested. Purified monocytes (3 x 106 per ml) were stimulated with 50 µg/ml pCRP and 20 µM ADP and allowed to adhere for 35 min. ADP was used to activate supplemented platelets. Subsequently, cells were washed extensively before cell adhesion was quantified by addition of a calorimetric phosphatase substrate (50 mM sodium acetate pH 5.0, 1% Triton X-100 and 40 mg of phosphatase substrate) and absorbance measured by 405 nm by spectroscopy after 30 min. We have previously demonstrated that upon binding to ADP-activated platelets pCRP undergoes transitional conformational changes 13, leading to increased expression of TNF, IL-1β, and IL-6 in CD14+ monocytes. (E) Expression of TNF, IL-6 and IL-1β in monocytes in flow cytometric assays using cytokine-specific antibodies as described in Supplementary Materials and Methods. Addition of C10M to the whole blood samples inhibits the CRP-dependent expression of the tested cytokines. Human heparinized whole blood was incubated with 50 µg/ml pCRP, 20 µM ADP, and C10M (1:100 molar ratio to CRP), respectively. Platelets in whole blood samples were stimulated by adding ADP where indicated. P values were calculated with ANOVA and Tukey's post-hoc test. n = 6, bars indicate mean ± SEM. **P <0.01, ****P <0.0001, ns not significant. (F) Representative examples of whole blood samples treated with pCRP and C10M as described above visualized by confocal fluorescence microscopy. Blood was treated as described above. ADP-activated platelets in heparin-anticoagulated whole blood. After RBC lysis, cells are transferred to µ-slides and subsequently embedded as single cell layers. Depicted are 3D reconstructions of multiple focal planes (Z-stack) at 20x magnification. The nuclei of whole blood leukocytes were stained with DAPI (blue) and TNF with anti-TNF-FITC (Mab11, green). Scale bar 50 µm.

Figure 4

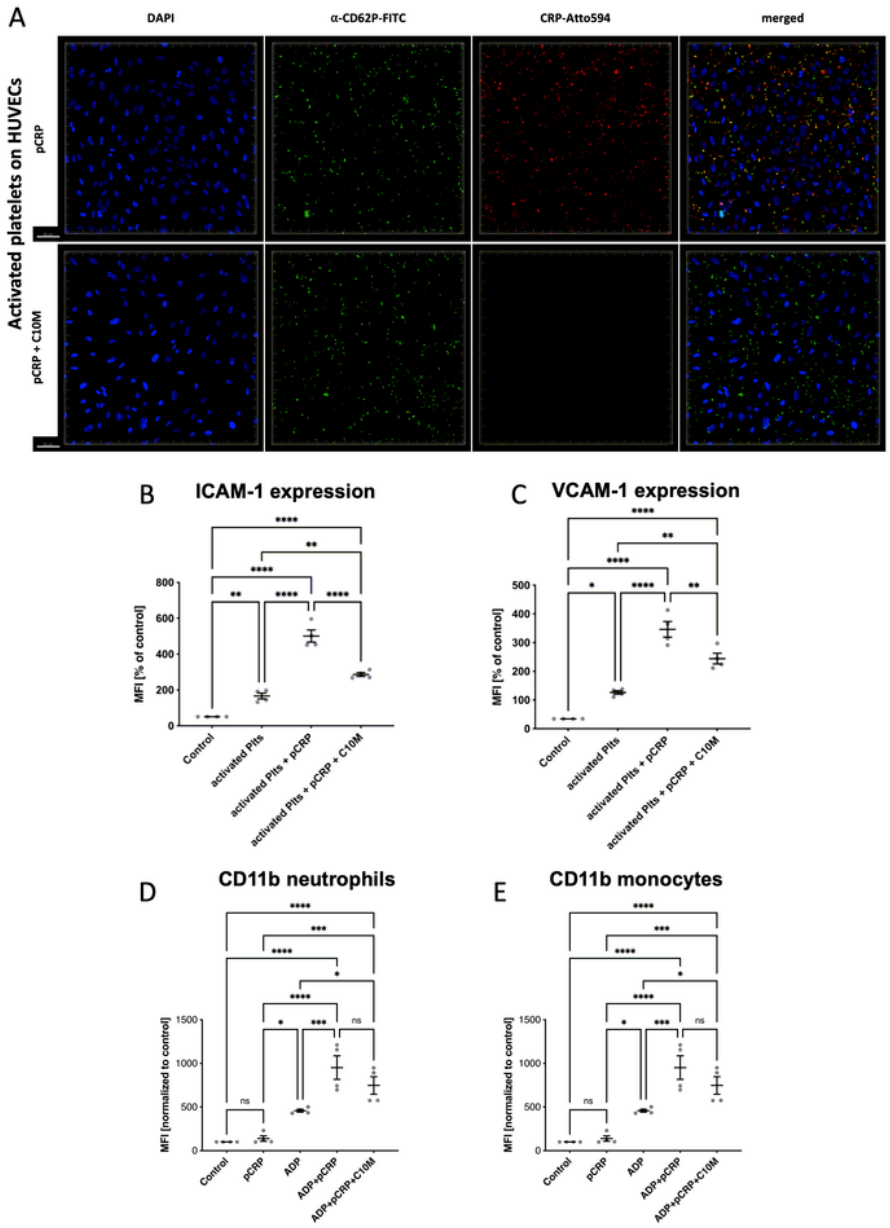

Figure 4

pCRP binding to ADP-activated platelets is inhibited by C10M, reducing adhesion molecule expression for leukocyte diapedesis in both endothelial cells and leukocytes, ROS formation and NET formation. (A) Confocal fluorescence microscopy of ADP-activated platelets bound to HUVEC mono cell layers. Platelets were isolated from citrated fresh human whole blood, stimulated with 20 µM ADP in PBS supplemented with calcium. 50 µg/ml pCRP-Atto 594 was added and incubated with and without C10M for 15 min at 37

°C, 5 % CO2. Anti-CD62P-FITC antibody was used to detect the platelets (green). Subsequently, stained platelet-CRP suspension was washed and added to HUVEC cell layers. HUVEC nuclei were counterstained with DAPI (blue). pCRP (Atto 594, red) colocalizes with platelets on the endothelial cells. When C10M was added simultaneously with pCRP-Atto 594, it inhibits CRP binding to platelets. Scale bar, 50 µm. Quantification of ICAM-1 (B) and VCAM-1 (C) expression on pCRP*/mCRP-activated HUVECs. Platelets were isolated from citrate-anticoagulated whole blood, washed and adjusted to 2 x 108 platelets/ml PBS supplemented with 13 mM calcium. Platelets were activated with 20 µM ADP and the designated platelet solutions were then incubated with 50 µg/ml pCRP and with or without C10M (1:100 molar ratio) for 15 min at 37 °C, 5 % CO2. HUVECs were incubated with CRP-platelet complexes and 20 % normal human serum in endothelial cell growth medium for six hours. ICAM-1 and VCAM-1 expression were measured by flow cytometry. C10M inhibits generation of pCRP* and thereby inhibits the induction of ICAM-1 and VCAM-1. Scatter plots of mean fluorescence intensity (MFI) results in flow cytometry are shown with results normalized to control = 100, mean ± SEM. P values were calculated with ANOVA and Tukey's post-hoc test. n = 4. *P <0.05, **P <0.01, ***P <0.001, ****P <0.0001. Expression of integrin subunit αM (CD11b) in neutrophils (D) and CD14+ monocytes (E) was accessed by flow cytometry as described previously 51. Human whole blood was incubated with 25 µg/ml pCRP or mCRP, 20 µM ADP and C10M, respectively. Subsequently, red blood cells were lysed and CD11b expression analyzed in neutrophils (CD16+, SSC high) and monocytes (CD14+, SSC low). Shown are scatter plots of MFI results in flow cytometry with results normalized to control = 100, mean ± SEM. P values were calculated with ANOVA and Tukey's post-hoc test. n = 6. *P <0.05, **P <0.01, ***P <0.001, ****P <0.0001, ns: not significant.

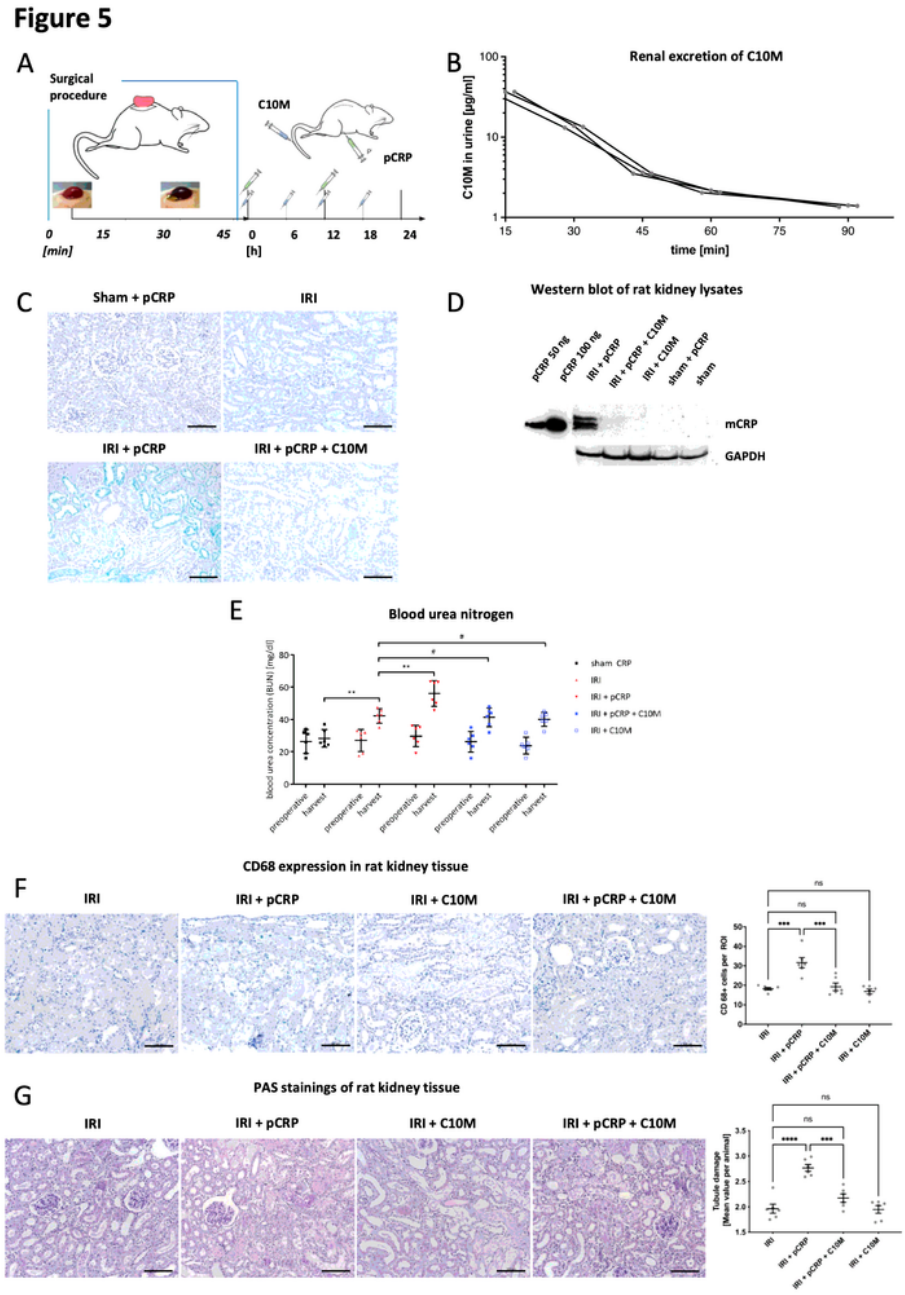

Figure 5

pCRP*/mCRP-driven exacerbation of renal ischemia reperfusion injury is reduced by C10M. (A) Depiction of the experimental protocol used for ischemic acute kidney injury. Male Wistar rats were subjected to IRI and received i.p. DPBS and pCRP twice (green syringe). C10M was i.v.-injected separately every 6 hours (blue syringe). (B) Renal excretion of C10M. C10M was i.v.-injected in the same setting described above. Urine was sampled by sterile puncture of the urinary bladder 15, 30, 45, 60, and 90 min after intravenous

application of C10M. Over 80 % of the applied C10M mass was excreted after 90 min. (C) Immunohistochemistry of rat kidneys subjected to IRI and i.p. pCRP application revealed distinct staining by anti-pCRP*/mCRP-9C9 antibody (green). C10M reduces the deposition of total CRP in the impaired tissue. No deposits in the non-ischemic tissue (sham). Exemplary stainings out of at least three are shown. Scale bars, 100 µm. (D) Tissue lysates of rat kidney were separated on SDS-PAGE and total CRP was identified with anti-CRP antibody (Clone 8). A band at the size of mCRP (~23 kDa) was detected in kidneys subjected to IRI and pCRP, but not in animals treated additionally with C10M. Representative results are shown. (E) Renal excretion is impaired by pCRP*/mCRP-driven tissue damage. Blood urea nitrogen (BUN) was utilized as surrogate marker for the excretion function of the kidney. Blood samples were taken before the surgical procedure (preoperative) and 24 hours after the procedure (harvest). (F) Immunohistochemical detection of transmigrated CD68+ cells in IRI kidneys. Representative results are shown. pCRP (25 µg/ml) increased the number of CD68+ cells transmigrated into injured renal tissue significantly, while C10M abolished these effects. Scale bars indicate 100 µm. Quantification of immunohistochemical results is shown on the right. Presented are mean cell counts per ROI in each animal (n = 6 per group). One-way ANOVA was used to compare treatments. # not significant, ***P <0.001. (G) Periodic acid-Schiff (PAS) stained kidney sections show increased damage after renal IRI in rats when pCRP was injected i.v. The tubulointerstitial injury was quantified by the loss of tubular brush border and by cast formation following an established protocol 52,53. Scale bars indicate 100 µm. Quantification of immunohistochemical results is shown on the right. Statistical analysis was performed with ANOVA and Tukey’s post hoc test. n = 6, **P <0.01, ***P <0.001, ns: not significant.

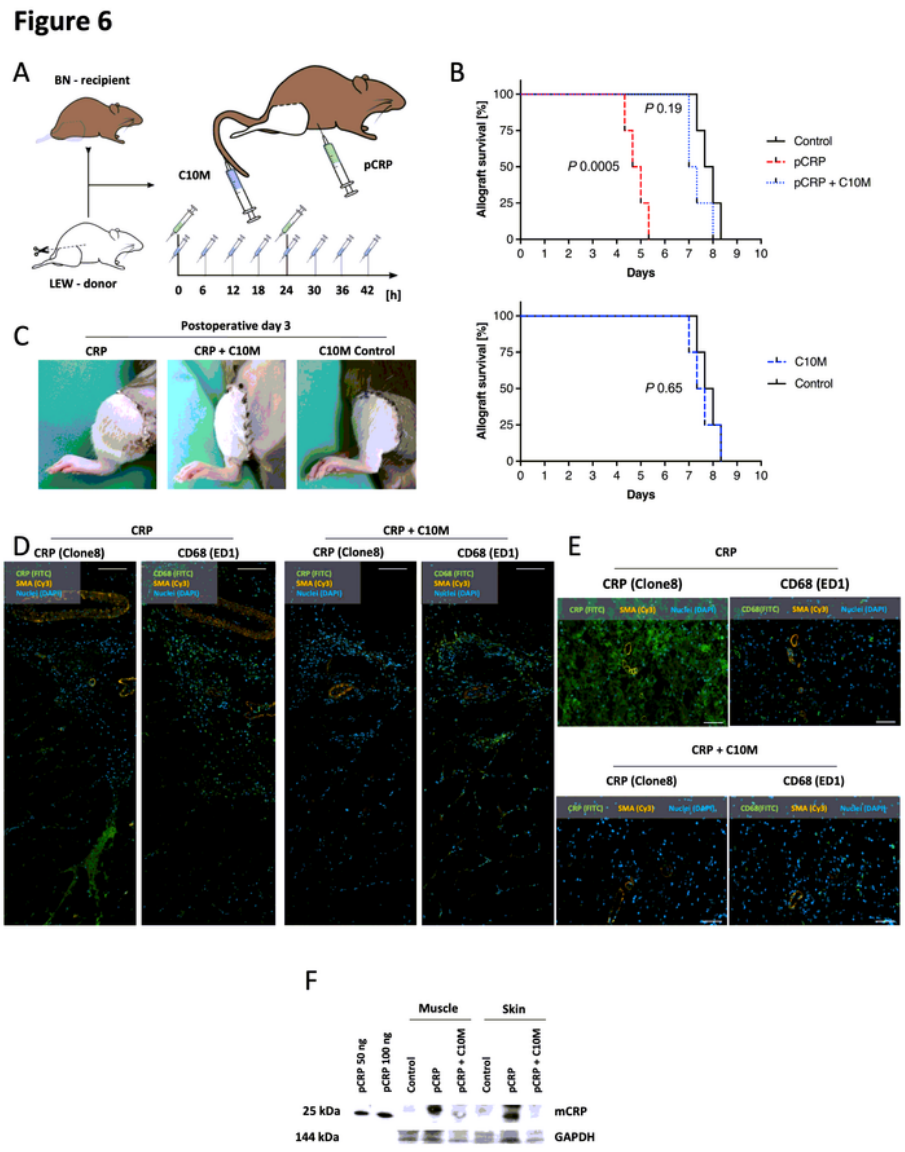

Figure 6

Compound C10M delays CRP-driven transplant rejection in a hindlimb transplantation model. (A) Experimental protocol of the acute vascularized composite allograft (VCA) rejection model in rats. Lewis (LW) rats served as hindlimb donors, fully mismatched Brown-Norway (BN) rats as recipients. Hindlimb rejection was assessed clinically and histologically. DPBS, pCRP (green syringe) and C10M (blue syringe) were injected i.p. and i.v., respectively. (B) Kaplan-Meier plots for control, pCRP, and pCRP + C10M (above)

and C10M vs control (bottom) treatment for total hindlimb allograft survival. Recipients were injected twice with PBS (control), 25 µg pCRP, or 25 µg pCRP + C10M per ml serum, respectively. C10M boli were applied i.v. at a 1:100 molar ratio pCRP/C10M postoperative every six hours for two days. Kaplan-Meier curves for different treatments were compared using log-rank test. Hindlimb survival interval was compared by Mantel-Cox log-rank test and was significantly reduced by pCRP administration (P = 0.0005, median survival control vs pCRP, 7.8 vs 4.8 days). C10M masks the CRP-accelerated hindlimb rejection (median survival 7.2 days). (C) Representative photographic examples of transplanted VCA hindlimb allografts. Shown are LW hindlimb transplants in orthotopic situ on BN recipients three days after transplantation. Rats receiving i.p. pCRP presented VCA with massive edema (left). C10M treatment masks pCRP-driven early graft rejection (middle). The depicted C10M control shows no clinical signs of rejection after five days but has no intrinsic effects (right). (D, E) Representative immunofluorescence microscopic pictures of sections from transplanted grafts reveal distinct signals (CF488, green) using anti-CD68 and anti-CRP antibodies, respectively. In C10M treated animals, significantly less CD68+ cells infiltrate the transplanted tissue. Scale bars, 100 µm. (D) Immunohistochemistry of transplanted muscle tissue revealed distinct CRP-deposition (green) in pCRP treated animals, but only minimal staining in rats treated additionally with C10M. Scale bars, 100 µm. (E) Immunohistochemistry of transplanted skin tissue revealed distinct CRP-deposition (green) in pCRP treated animals, but no staining in rats treated additionally with C10M. Scale bars, 100 µm. (F) Exemplary tissue lysates of skin and muscle probes separated on SDS-PAGE are depicted. Total CRP was identified with an anti-CRP antibody (Clone8).

Figure 7

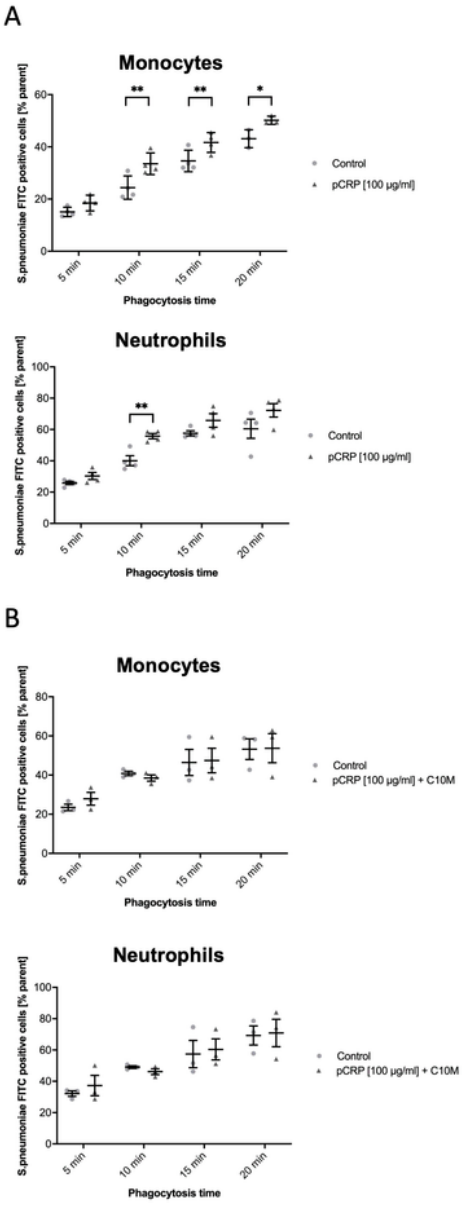

Figure 7

Opsono-phagocytosis of S. pneumoniae serotype 27 is not compromised by C10M. (A) Phagocytosis of pCRP-opsonized heat-killed and FITC-labeled S. pneumoniae by monocytes and neutrophils serves as exemplary phagocytosis assay. Whole blood samples of healthy volunteers were incubated with targets with and without pCRP (100 µg/ml), processed as described in Supplementary Materials and Methods and then measured by flow cytometry. Scatter plot shows phagocytic index (percentage of target positive

cells of subtype / all cells of subtype) of un-opsonized (control, light-grey dots) and CRP-opsonized targets (dark-grey triangles) after 5, 10, 15, and 20 min, respectively. Targets were incubated with pCRP in the presence of calcium for 30 min, 37° C. Mean ± SEM are indicated. P values were calculated using ANOVA and Tukey's post hoc test. n = 4, **P < 0.01, *P < 0.05. (B) Experiments as described in (A) were repeated but with targets incubated with pCRP (100 µg/ml) and C10M (1:100 molar ratio) for 30 min, 37 °C. Mean ± SEM are indicated. n = 4, **P < 0.01, *P < 0.05.

Figure 8

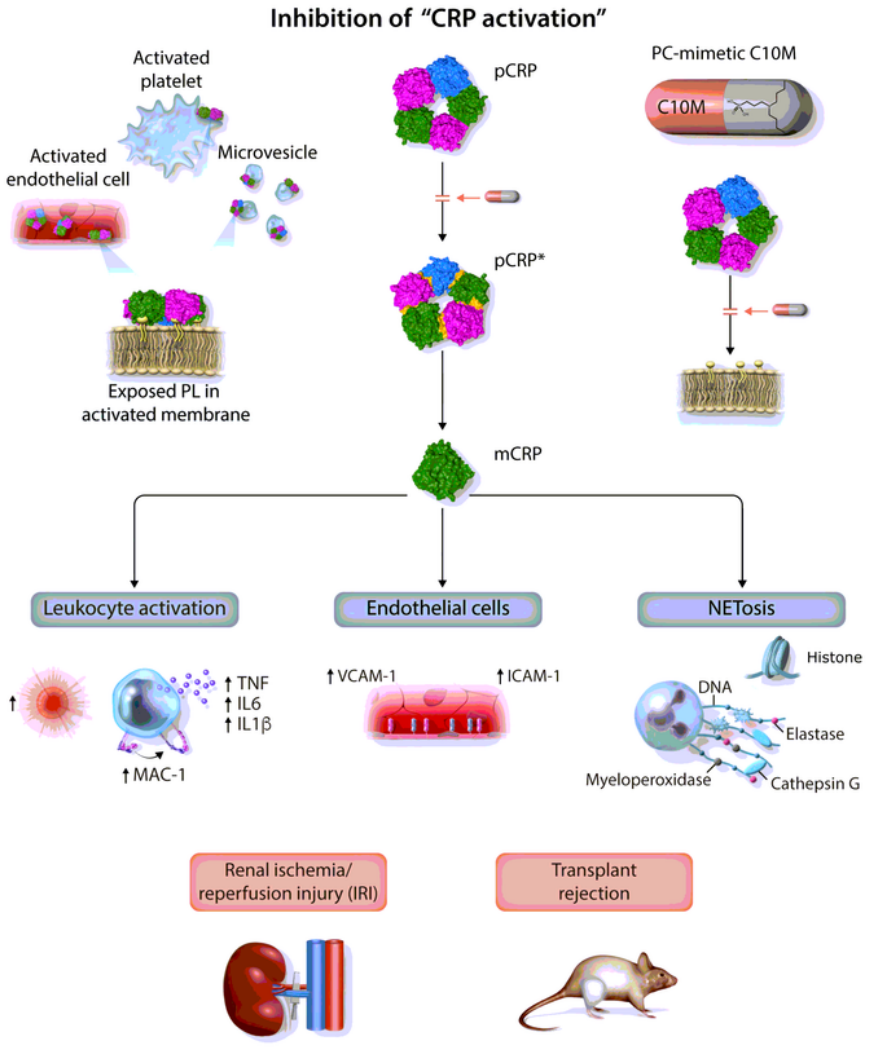

Figure 8

Schematic model of “CRP activation” and C10M’s in-vitro and in-vivo anti-inflammatory effects. Exposed phospholipids (PL) in activated cell membranes (e.g. endothelial cells or platelets) or microvesicles contain PC and PE head groups, which bind to the PC/PE binding sites on the B-face of pCRP thereby anchoring pCRP to the membrane surface. Once bound to the activated membrane, pCRP dissociates into pCRP* and ultimately mCRP. This “CRP activation” results in the activation of leukocytes and endothelial cells as well as NETosis and contributes substantially to renal ischemia/ reperfusion injury (IRI) and transplant rejection. Administration of C10M prevents “CRP activation”, the consequent pro-inflammatory cellular effects and reduces renal IRI and transplant rejection.

Supplementary Files

This is a list of supplementary files associated with this preprint. Click to download.

- ZelleretalSupplementaryInformation.docx